FINAL REPORT

Surf-zone Underwater Robotic Demonstration Platform

SERDP Project MR-2325

JANUARY 2014

Terri Wirth Koepenick
Applied Research Associates, Inc.

Distribution Statement A
This document has been cleared for public release

SERDP
DOD ▪ EPA ▪ DOE

This report was prepared under contract to the Department of Defense Strategic Environmental Research and Development Program (SERDP). The publication of this report does not indicate endorsement by the Department of Defense, nor should the contents be construed as reflecting the official policy or position of the Department of Defense. Reference herein to any specific commercial product, process, or service by trade name, trademark, manufacturer, or otherwise, does not necessarily constitute or imply its endorsement, recommendation, or favoring by the Department of Defense.

Table of Contents

Abstract....1
Objective....3
Background....6
Materials and Methods....9
Biomimetic Hull Design....9
Archimedes Screw Design....15
Results and Discussion....18
Biomimetic Hull Design: Fluent CFD Modeling....18
Biomimetic Hull Design: Flow Channel Testing....20
Archimedes Screw Design and Testing....23
Conclusions and Implications for Future Research....30
Biomimetic Hull Conclusions....30
Archimedes Screw Conclusions....30
Overall Conclusions and Next Steps....31
Literature Cited....33
Appendix A: Biomimetic Hull Test Plan....34
1. Introduction....34
1.1. Biomimetic Hull Overview....34
1.2. Purpose....34
2. Test Design....34
2.1. General test setup....34
2.2. Variables....34
2.2.1. Testing Variables....34
2.2.1. Testing Data....34
2.3. Test hull description....35
2.4. Test Fixture....35
3. Test procedures....35
3.1. General test procedure....35
3.2. Data analysis....36
Appendix B: Archimedes Screw Test Plan....37
1. Introduction....37
1.1. Archimedes Screw Overview....37
1.2. Purpose....37

Copyright Applied Research Associates, Inc., 2014

2. Test Design 37
2.1. General test setup 37
2.2. Variables 37
2.2.1. Test variables 37
2.2.2. Test data 37
2.3. Test screws description 38
2.4. Test rig description 38
2.5. Test bed description 38

3. Test procedures 38
3.1. General test procedure 38
3.2. Auxiliary tests 39
3.3. Data analysis 39

Appendix C: Shell CFD Test Data 40

Appendix D: Archemedis Screw Test Data 46

Appendix E: Archemedis Screw Test Data 48

List of Figures

Figure 1: 3D Model used for CFD Analysis 4

Figure 2: 3D Printed Shell for Water Testing 4

Figure 3: Optimized Archimedes Screw Design 5

Figure 4: Forces acting on screw 7

a) Deadweight and drawbar forces 7

b) Forces acting on mean helix angle 7

c) Forces acting at base diameter 7

Figure 5: Segmentation of Limulus Polyphemus 10

Figure 6: Limulus Polyphemus One 11

Figure 7: Limulus Polyphemus Two 11

Figure 8: Baseline Model with Neutral Opisthosoma 11

Figure 9: 3D Model Smooth 12

Figure 10: 3D Model Indented Top 12

Figure 11: Baseline 13

Figure 12: Smooth 13

Figure 13: Indented Top 13

Figure 14: Flow Channel Test Fixture 14

Copyright Applied Research Associates, Inc., 2014

Figure 15: Experimental Setup 14
Figure 16: Model attached to bracket 15
Figure 17: Testing configuration 15
Figure 18: Single-start Archimedes Screw 15
Figure 19: Experimental Test Bed and Platform.....15
Figure 20: Parametric Design 15
Figure 21: Flow Pathlines for Neutral Opisthosoma at 10m/s.....18
Figure 22: Velocity Vectors at 25m/s 18
Figure 23: Velocity Vectors at 25m/s 18
Figure 24: Flow Pathlines for Smooth Shell 19
Figure 25: Velocity Vectors for Smooth Shell 19
Figure 26: Drag (N) for Four Simulated Models at Five Flow Velocities.....20
Figure 27: Lift (N) for Four Simulated Models at Five Flow Velocities.....20
Figure 28: Drag (N) for three models at three flow velocities.....22
Figure 29: Lift (N) for three models at three flow velocities.....22
Figure 30: Four Screws: A, B, C, and D (from left to right).....23
Figure 31: Screw D Tested in Wet Sand 24
Figure 32: Power Consumption in Wet Sand.....25
Figure 33: Screw D Tested in Rocks 25
Figure 34: Power Consumption in Pebbles 26
Figure 35: Water Testing 26
Figure 36: Power Consumption in Water 27
Figure 37: Platform Velocity in Water 27
Figure 38: Three tested screw depths below test platform (1, 2, 3 from left to right).....28
Figure 39: Skid Testing Configuration 1 (skid at axis of rotation) 28
Figure 40: Shallow Water Testing.....29
Figure 41: Design bottom view 31
Figure 42: Design front ISO view 31
Figure 43: Flow Pathlines for Baseline Shell with Flow Perpendicular to Shell at 25m/s.....40
Figure 44: Velocity Vectors for Baseline Shell with Flow Perpendicular to Shell at 25m/s.....41

Copyright Applied Research Associates, Inc., 2014

Figure 45: Flow Pathlines for Indented Shell at 10m/s 41
Figure 46: Velocity Vectors for Indented Shell at 10m/s.....42
Figure 47: Flow Pathlines for Treaded Vehicle at 0.5m/s 42
Figure 48: Velocity Vectors for Treaded Vehicle at 0.5m/s 43
Figure 49: Drag (N) for Four Simulated Models for Flow Velocities from 0 to 1.5m/s.....43
Figure 50: Lift (N) for Four Simulated Models for Flow Velocities from 0 to 1.5m/s.....44
Figure 51: Lift (N) for Four Simulated Models for Flow Velocities from 0 to 10.5m/s.....44
Figure 52: Moment (N•m) for Four Simulated Models at Five Flow Velocities 45
Figure 53: Moment (N•m) for Four Simulated Models for Flow Velocities from 0 to 1.5m/s.....45
Figure 54: Coefficient of lift for three models at three flow velocities.....46
Figure 55: Coefficient of lift for three models at three flow velocities.....47
Figure 56: Platform Velocity by Screw Type for Wet Sand 49
Figure 57: Platform Velocity by Screw Type for Pebbles.....50

List of Tables

Table 1: Comparison of Fluent CFD and Flow Channel Test of Lift and Drag 21
Table 2: Screw Parameters for Four Designs.....23
Table 3: Robotic Sub-system Components from COTS Manufacturers.....32
Table 4: Comparison of Fluent CFD and Flow Channel Lift and Drag Coefficients.....46
Table 5: Wet San Test Results 48
Table 6: Pebble Test Results 49
Table 7: Water Test Results.....51

Copyright Applied Research Associates, Inc., 2014

List of Acronyms

ARA	Applied Research Associates, Inc.
ASTM	American Society for Testing and Materials
CFD	Computational Fluid Dynamics
COTS	Commercial Off the Shelf
DoD	Department of Defense
EM	Electromagnetic
ESTCP	Environmental Security Technology Certification Program
mm	Millimeter
MR	Munitions Response
SERDP	Strategic Environmental Research and Development Program
SURDP	Surf-zone Underwater Robotic Demonstration Platform
SZ	Surf-zone
USGS	United States Geological Survey
UWMM	Underwater Military Munitions
VSW	Very Shallow Water
VI	Virtual Instrument
3D	Three-Dimensional

List of Keywords

- Archimedes Screw - helical flange surrounding a central cylindrical shaft
- Biomimetic - study of the structure and function of biological systems as models for the design and engineering of materials and machines
- Computational Fluid Dynamics - use of high-speed computers to numerically solve the complete nonlinear partial differential equations governing viscous fluid flows
- Surf Zone - region where surface waves actively dissipate energy due to depth-limited wave breaking, classified by the U.S. Navy as 0 – 10 feet
- Towing Capability – for the purposes of this study towing capability is the measurement of the tractive force that the Archimedes screw drive can impart in a specific medium
- Very Shallow Water - corresponds to the oceanographically defined inner shelf where fluid motions can be dominated variously by wave, tides, or low-frequency currents, classified by the U.S. Navy as 10 – 40 feet

Copyright Applied Research Associates, Inc., 2014

Abstract

Objective

The Department of Defense (DoD) is faced with the challenge of identifying and characterizing locations in U.S. coastal and inland waters where underwater military munitions (UWMM) are present and develop safe and cost-effective means to remediate these sites as an important step towards comprehensive range clearance. The Strategic Environmental Research and Development Program (SERDP) Munitions Response (MR) Program Area has identified the need to develop technologies to detect, classify, and retrieve UWMM leftover from past military training and weapons testing activities.

The underwater environment is one of the most challenging and dynamic operating environments for both man and machine making UWMM location and recovery especially difficult. One of the more critical and technically challenging environments, as identified by the 2007 SERDP and ESTCP Final Report (Technology Needs for the Characterization, Management, and Remediation of Military Munitions in Underwater Environments), is the surf-zone[1].

ARA studied two key engineering concepts that directly affect the ability of a robotic system to operate in the surf-zone; platform hull shape and propulsion. To address platform hull shape ARA undertook a research and technical study of an existing arthropod's (horseshoe crab) carapace as a biomimetic representation for the hull shape of a robotic system. This work was used to develop a hydro-dynamically advantageous shape for a robotic system. To address locomotive factors ARA completed a research and technical study based on an Archimedes screw drive as the mode of propulsion to assess platform traction and mobility in the near shore environment; very shallow water (VSW) and surf-zone (SZ).

Technical Approach

An applied research approach was used to study stability, mobility, and traction. To study stability a horseshoe crab's carapace served as the basis for a biomimetic hull shape that would theoretically provide the appropriate balance between lift and drag for a robotic platform operating in the VSW/SZ. The use of a biomimetic hull as a hydrodynamic design shape was chosen in order to direct water flow and wave energy in such a way as to aid in tractive potential and stability. Several biomimetic hulls were modeled and underwent simulated and empirical testing in a water channel. The empirical testing was used to validate the data obtained from the Computational Fluid Dynamics (CFD) simulations used to identify a more effective hull shape.

To study mobility and traction a propulsion system based on an Archimedes screw drive was used. A drive design based on an Archimedes screw was chosen because of its ability to operate in various mediums with varying flow rates. A test bed was designed and assembled in order to measure the speed, power consumption created by the screw drive when interacting with various mediums. Several screw drive designs with different design parameters were empirically tested to record efficacies in a range of mediums, including water, sand, and pebbles.

Copyright Applied Research Associates, Inc., 2014

Results

CFD analysis and empirical testing has demonstrated the ability for a robot to operate in the VSW/SZ. A shell was optimized to reduce drag and lift. Fluent modeling was used to compare different potential hull shapes for optimizing the design of a future robot. The horseshoe crab shells (Limulus Polyphemus) was used a baseline model. Two other similar shapes where modeled with improved drag reduction characteristics. The CFD modeling confirmed that the smooth shell had the lowest drag in comparison to all other tested hull shapes

Empirical flow testing was conducted to confirm the results of the Fluent CFD analysis. Three 3D printed hulls were tested at the same flow rates as CFD modeling for comparison. The experiments confirm that the smooth hull had the lowest drag of any shape tested. There is also strong agreement between the data from the Fluent CFD modeling and the results of the empirical experiments. This gives high confidence in the Fluent results. All testing confirms that it is possible to design a hull shape to improve stability in the dynamic wave conditions found in the VSW/SZ.

An ideal Archimedes screw drive was determined and is sufficient to be used across different mediums; such as sand, water, and gravel. Testing of multiple screw profiles was conducted in a custom test bed capable of holding the above mediums. The ideal screw outperformed all of the designs in every experiment.

Benefits

Results of this research lay the groundwork for the follow-on development of a prototype unmanned Surf-zone Underwater Robotic Demonstration Platform (SURDP) capable of operating in and around the near shore environment. The SURDP will enable the DoD to conduct detailed and comprehensive underwater surveys in the VSW/SZ by providing a platform with the necessary stability and mobility to employ the sensors required to locate and classify UWMM.

Copyright Applied Research Associates, Inc., 2014

Objective

The near shore environment is one of the most challenging and dynamic environments for both man and machine making UWMM location and recovery especially difficult. Current practices employing military explosive ordnance disposal (EOD) or contract divers for manual location and retrieval of UWMM is dangerous, time-consuming, resource intensive, and costly. While divers provide a tremendous capability to locate and retrieve UWMM, manned operations in the VSW/SZ are greatly affected by local environmental conditions. In addition to human safety and environmental considerations, operating a dive station demands significant time and resources due to the large logistical footprint required to support the number of divers and equipment required for even a small remediation operation. As a result, the SERDP has identified the need to develop robotic technologies to detect and classify discarded or unexploded ordnance in the VSW/SZ.

Significant developmental efforts have been made to investigate sea-floor crawling robots, but they usually involve "water-proofing" a standard ground robot and attempting to operate it underwater. This design concept ignores the unique challenges of the near shore environment. First, the aquatic floor is a significantly different medium from that of dry land. Standard ground mobility components like tracks and wheels do not have the same efficacy in the water. Second, the VSW/SZ is a highly dynamic environment where water flow and wave action exert strong kinematics that can severely impact underwater vehicles not designed to withstand these unique conditions. Standard ground robots usually end up being pushed around, destabilized, and/or toppled[2]. The forces within the VSW/SZ create a mobility and traction problem that leads to instability, and sensor and navigational challenges. To address the factors that directly affect the ability of a robotic system to operate in the VSW/SZ, ARA studied two key engineering design concepts; platform hull shape and propulsion.

To study platform stability in the VSW/SZ, ARA used a biomimetic approach to evolve a hydrodynamic hull shape that would take advantage of the kinematics in the VSW/SZ to provide an increased down force to increase tractive potential. ARA hypothesized that a robotic hull shape based on the shell of a horseshoe crab will allow hydrodynamic forces in the VSW/SZ to assist in the ability to station keep and maneuver without the need for excessive weight or a complex propulsion system to achieve platform stability and traction. Based on its natural habitat with the near shore environment a horseshoe crab carapace was chosen as a biomimetic representation for the hull shape to answer the following questions:

- Can a biomimetic hull design provide better stability in the dynamic wave conditions found in the VSW/SZ?
- Is the required scale of this hull design sufficient for carrying a usable payload and other system components?
- What are the maximum flow vectors for which the biomimetic hull can remain effective?

What are the resultant forces from those maximum flow vectors?

"Owing to crawler size, it is unexpectedly susceptible to being moved by waves within the shore-break (or across the surf zone with increased payload drag). This requires swimmer assistance for re-orientation and visual checks." (Gallagher & MacMahan 2007)

Copyright Applied Research Associates, Inc., 2014

Computational Fluid Dynamics (CFD) modeling and empirical water channel testing was used to compare various biomimetic hull shapes (figures 1 and 2) and how they respond to flows of varying speeds and orientations. The result of this research was the design shape for an advantageously hydrodynamic hull for the SURDP.

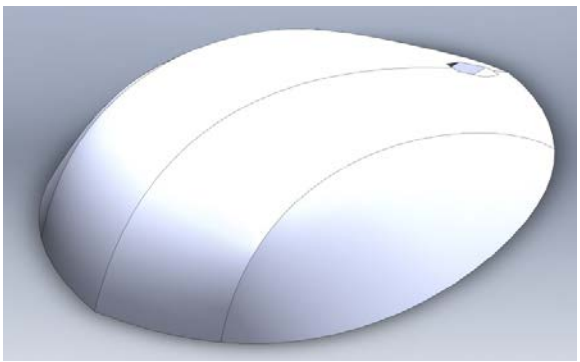

Figure 1: 3D Model used for CFD Analysis ***Figure 2: 3D Printed Shell for Water Testing***

To study traction and mobility in the VSW/SZ, ARA completed a technical study based on an Archimedes screw drive as the mode of locomotion. ARA hypothesized that an Archimedes screw with optimal geometry could provide the tractive force in a suspended solid to propel a robotic system. Archimedes screw drives have been successfully used on larger underwater robots, such as those found in the deep sea mining industry[3], but it has not been widely applied to a robotic system in the near shore environment.

A test bed was designed and assembled in order to measure the speed, power consumption, and displacements created by an Archimedes screw drive when interacting with various mediums. Several drive designs with different flange heights, depths, and types were empirically tested to record efficacies in a range of mediums, including water, sand, and pebbles to answer the following questions:

- Can the Archimedes screw drive be scaled appropriately for a small to medium robotic system?
- What performance characteristics (speed, efficiency, tractive force) would this system provide?
- How will the system perform across a variety of medium?
- Will the proposed system provide efficient short-distance swimming capabilities? If not, what is the trade-off between swimming and traction?

The result of this research was the optimized geometry (figure 3) for an Archimedes screw that would provide good tractive force on the aquatic floor and as a swimming thruster, as well as the operational speed and torque requirements of the driving motors for the SURDP.

Copyright Applied Research Associates, Inc., 2014

Figure 3: Optimized Archimedes Screw Design

Copyright Applied Research Associates, Inc., 2014

Background

The DoD is faced with the tremendous challenge of identifying and characterizing locations in U.S. coastal and inland waters where UWMM are present and develop safe and cost-effective means to remediate these sites. Many active and former defense sites have weapons and training ranges that include areas located in or adjacent to coastal or inland bodies of water. Some of these ranges lie in VSW and SZ regions of the coastline. While the location of these ranges may be known, little information is available on the location, type, or condition of the UWMM that may exist at these sites.

Despite advancements in the field of robotics there currently exists no autonomous system that can reliably detect and classify UWMM in the VSW/SZ. Existing platforms cannot maintain positional accuracy or effective operability due to the water flow and wave action, which significantly impacts their ability to conduct reliable searches to the appropriate confidence level or to complete the mission without becoming disabled. This technology gap largely exists because current systems focus on adapting ground based technology to the VSW/SZ, which is not well suited to this environment due to constraints associated with stability, mobility, and traction.

Design teams attempting to address stability problems brought on by operating in the VSW/SZ have tried a number of different approaches. One common approach is to increase the mass of the platform to generate enough traction with the aquatic floor to maneuver with standard locomotive designs. While this approach normally increases the stability of the platform, it does so at the cost of endurance and mobility in more viscous mediums (silt, mud, or muck). Many previous attempts at ground crawling platforms in the near shore environment have had limited success because of the types of propulsion used. Classic modified ground propulsion systems, like tracks and wheels, do not give the same kind of traction in the stratum found in VSW/SZ that they provide on land.

A body in a fluid flow experiences three primary forces. First, buoyancy causes an upward force that can be influenced by adding or subtracting weight and volume to the object. Next, surface friction drag creates a shearing force in the direction of flow along the surface of the body. This surface drag creates a positive moment pushing up on the leading edge of the object. The last primary force is pressure drag, caused the fluid's momentum change over the body. Pressure drag is highly variable based on geometry. Depending on the incident angle of oncoming flow the surface of the object can direct forces to drive the front end down or backwards (with the flow) adding to the friction drag. Depending on the geometry of the aft end, flow separation can be encouraged or discouraged resulting in an aft end pressure distribution that is stronger or weaker to counter, balancing the forward pressure distribution.

Significant research has been done to model robotic systems after biological sources because of the millions of years of biological success that can be utilized to increase performance characteristics or functionality in specific operating environments. While many animals live and thrive in the near shore environment, the horseshoe crab is particularly relevant. The horseshoe crab successfully balances the main forces found underwater, even in the volatile SZ as seen in

Copyright Applied Research Associates, Inc., 2014

their procreation behaviors[4]. The unique hydrodynamics of the horseshoe crab's shell creates enough down force for it to use its legs to maneuver, but not so much that it is permanently affixed to the bottom. The simplicity of its shape perfected over approximately 500 million years of evolution makes this a natural choice as a biomimetic representation for a VSW/SZ robotic system.

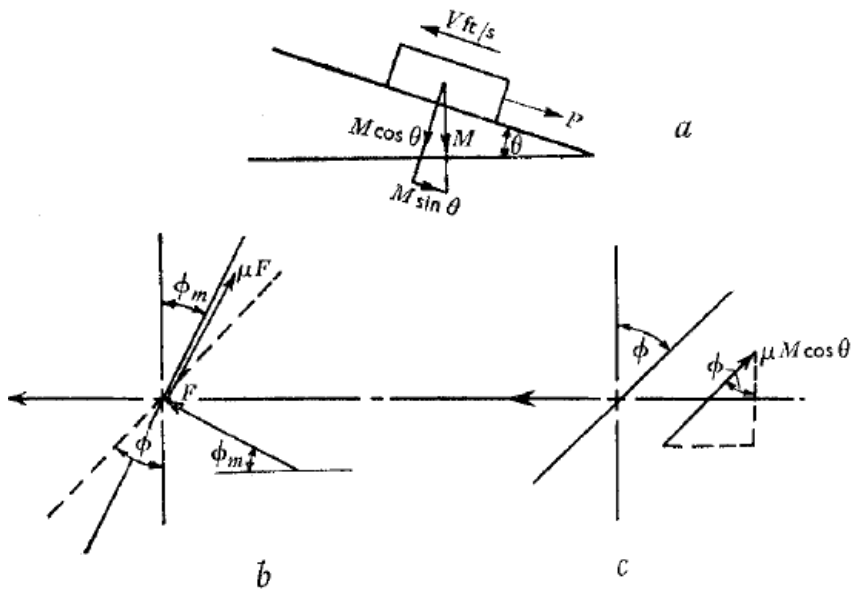

Figure 4: Forces acting on screw

a) Deadweight and drawbar forces

b) Forces acting on mean helix angle

c) Forces acting at base diameter

In addition to being stable in the VSW/SZ a robotic system needs to be able to provide efficient locomotion. Archimedes screw drives are especially well suited for propulsion in suspended solids due to their large tractive force potential as well as their high efficiency in a variety of mediums and flow rates. For a robotic system, the tractive force (figure 4) is the force that the screw can impart to the medium and is divided into two regimes; the amount of force required to break static equilibrium, and the force that the screws impart to the medium to maintain forward motion. The tractive force achieved is largely dependent on screw geometry and the conditions of the medium. Additionally, when screw velocity is substantially increased it can serve as a swimming thruster allowing greater mobility for a near shore robotic system.

Archimedes screw propulsion has been studied in the Soil Laboratory at IHC Merwede Kinderdijk, the Netherlands for the purpose of deep sea mining to determine slippage, motion behavior, adhesion, and bulldozer effects at the front side of the screws[5]. This study was done for a very large scale vehicle that required sufficient buoyancy (from cylinder volumetric

Copyright Applied Research Associates, Inc., 2014

displacement) to avoid burying itself in the bottom and offset the tremendous weight of its associated mining equipment.

The intent of the research was to design and investigate the use of a biomimetic hull shape and an Archimedes screw drive as the basis for the development of a robotic system that can operate effectively in the near shore environment. The research was used to test and characterize two enabling technologies so that a conceptual design for the SURDP could be developed based on validated data. This design engineering will help to reduce the risk of the SURDP development by ensuring that the basic parameters of the design are understood and are improvements upon existing platforms performance characteristics. ARA expects that the SURDP will be both inherently stable in dynamic wave environments and well-suited to traverse the varied mediums of the near shore environment.

After gaining in-depth sense of platform design and performance a trade study was completed on the availability of Commercial Off the Shelf (COTS) components and those requiring fabrication to outline the expected scale and development cost for a prototype SURDP system.

Copyright Applied Research Associates, Inc., 2014

Materials and Methods

Biomimetic Hull Design

Biomimetic hull design research was initiated with a literature review to gain a better understanding of the hydrodynamics of the horseshoe crab shell and the physical forces encountered in the VSW/SZ.

On wave-swept rocky shores, maximum water velocities have been observed in the range of 20 to 24m/s [6]. Typical water velocities are in the range of 0.5 to 10m/s. These values were used to determine maximum nominal flow rates to be simulated in the CFD analysis and during empirical water channel testing.

While no existing research was found that directly modeled drag and lift of a horseshoe crab shell in the near shore environment, several relevant papers were discovered which provided a greater understanding of the hydrodynamic effects of the arthropod's surface features. A series of papers by Mark Denny et al., of Stanford University, analyzed a similar shell shape in a similar environment. Denny studied limpets both in the lab and in their natural SZ environment to assess the impact of their shell's hydrodynamics on survivability. The apex of a limpet's shell is displaced anteriorly to form a plough that faces into the direction of flow[7]. Denny's studies conclude that limpet shells are not optimized for hydrodynamics, but are sufficient for survivability.

The numerous papers detail the hydrodynamic properties that would optimize the shell for survivability in the SZ. When the apex is displaced posterialy to form a wedge and is oriented downstream, both lift and drag are reduced. In this orientation, these shapes experience a substantial reduction in fluid dynamic drag at velocities above the abrupt transition from a laminar to a turbulent boundary. The shell shows a sudden 40% reduction in drag at a water velocity of 1.6 m/s, a velocity that is commonly encountered on wave-swept shores[8]. Additionally, their imperfect surface acts like a golf ball to induce a transition to turbulent flow at lower than expected velocity, which in-turn reduces drag. If caught broadside by a large wave the 'optimal' limpet would survive nearly five times better than the natural one. When the apex of the cone is downstream, the reduced lift coefficient and drag result in a lower tensile stress and sheer stress than if oriented upstream[9]. Their work, validated our analysis approach, and provided empirical measurement of relevant environmental parameters (flow properties).

Other papers reviewed at the start of the project provided insight into the biological and hydrodynamic benefits of various horseshoe crab shell structures (figure 5), such as the anterior spines ("Functional significance of spines in the Pennsylvanian horseshoe crab Euproops danae", Daniel C. Fisher, 1977), hinge and shell ridges ("Influence of Ambient Flow Around the Horseshoe Crab Limulus polyphemus on the Distribution and Orientation of Selected Epizoans", Joanne Dietl et al., 2000), and the anterior lip of the shell ("Observations on the Swimming, Righting, and Burrowing Movements of Young Horseshoe Crabs, Limulus polyphemus", E.D.Vosatka, 1970). The literature review helped focus design and optimization considerations to areas and characteristics that had potential noticeable effects on its hydrodynamic profile. The body design of Limulus prevents it from swimming right-side-up. When the animal swims, it

Copyright Applied Research Associates, Inc., 2014

assumes an inverted position[10]. The shell is so optimally designed to create down force when settled in the sand that it must swim inverted to maintain flight. The acceleration in the flow over the dorsal surface is in accordance with Bernoulli's principle. The pressure gradient steepens from the anterior to the posterior of the carapace and escalates the turbulence in the wake[11]. Much like the limpet shell of Denny's studies, the horseshoe crab's features reduce drag by inducing a transition to turbulent flow over the dorsal region of the shell.

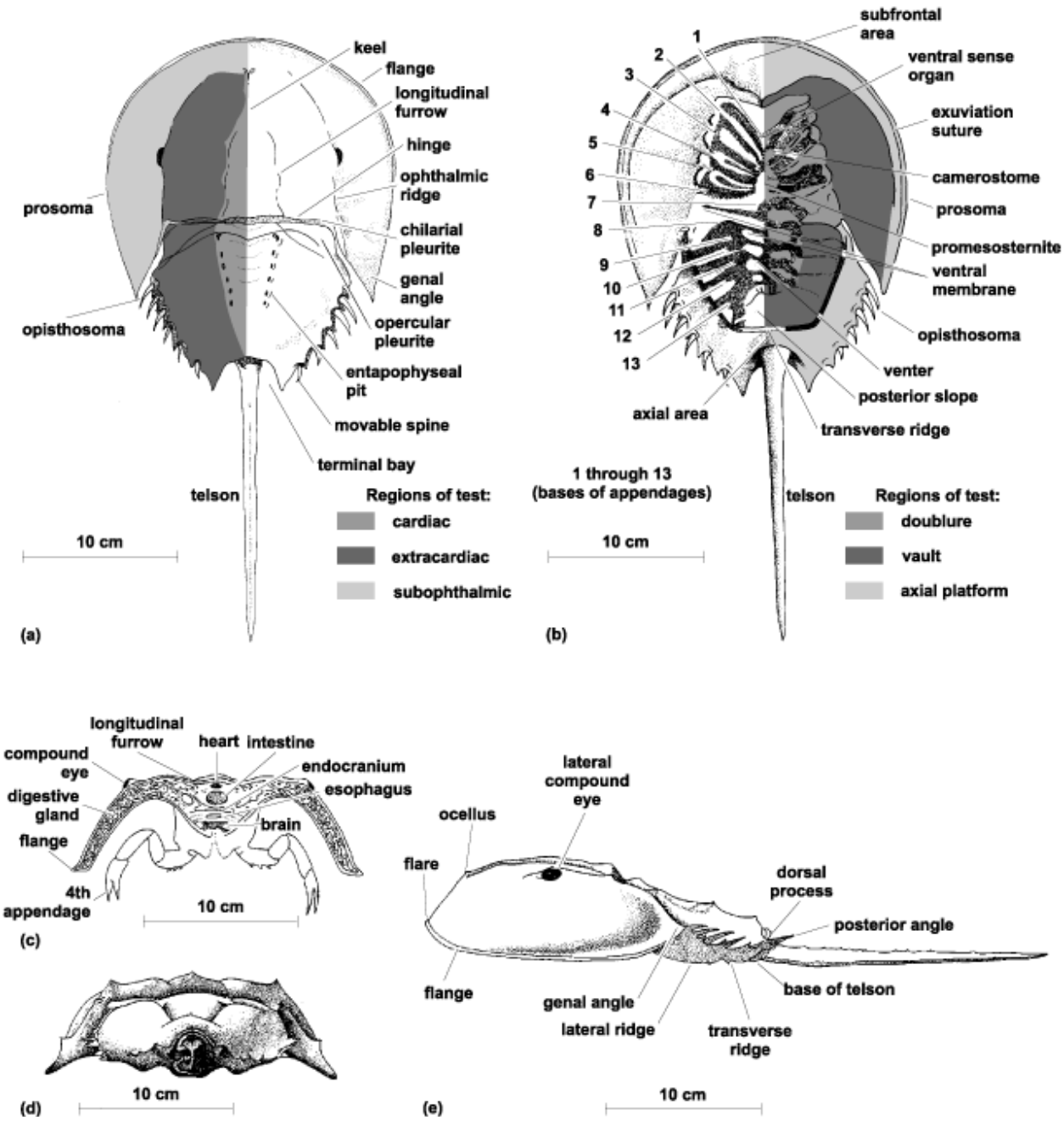

Figure 5: Segmentation of Limulus Polyphemus

A three-dimensional (3D) model spiral development process was used to develop biomimetic hull shapes for testing. Two adult horseshoe crab shells (Limulus Polyphemus) were purchased (figures 6 and 7). While each shell had similar appearances and surface features, the shells had visibly noticeable differences, possibly due to sexual dimorphism.

Figure 6: Limulus Polyphemus One

Figure 7: Limulus Polyphemus Two

The shell with the higher vertical profile (figure 7) was selected for 3D computer modeling since it would provide a greater internal volume to integrate a sensor package and propulsion components when scaled for use as a hull for a robotic system. The chosen shell was subjected to structured light scanning to create a 3D computer model of the surface. The 3D computer mesh from the light scan was loaded into SolidWorks and used to produce a simplified, longitudinally symmetric 3D computer model (Figure 8) for follow-on CFD analysis. This computer model was also used as the baseline to compare other design options against.

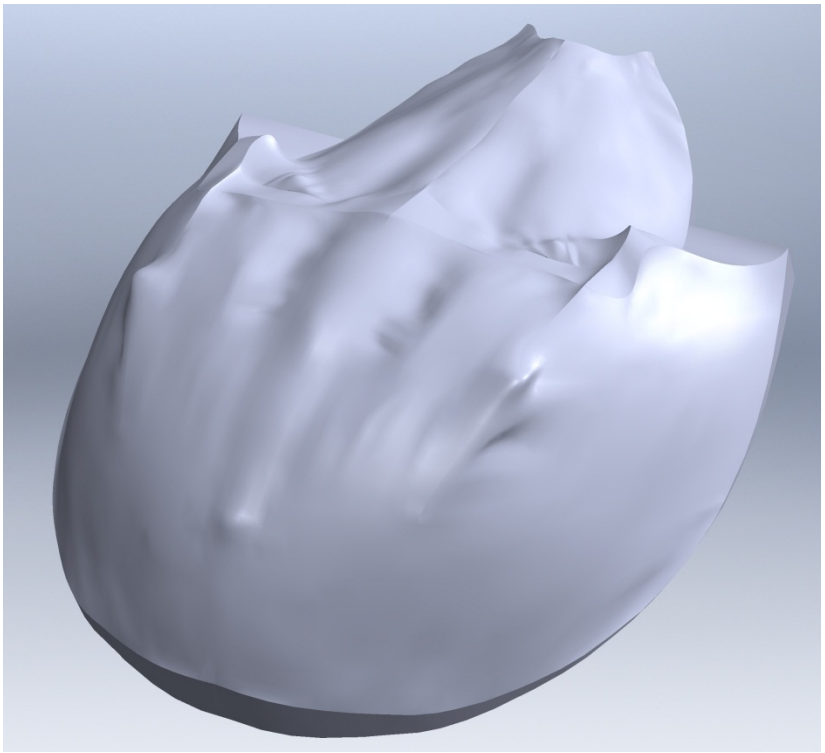

Figure 8: Baseline Model with Neutral Opisthosoma

Copyright Applied Research Associates, Inc., 2014

Based on conclusions drawn from the literature review, and visual observations of the shell, it was speculated that the orientation of the opisthosoma (anterior section of the horseshoe crab) might provide hydrodynamic benefits. The baseline 3D computer model was analyzed in Fluent in four orientations: neutral opisthosoma, opisthosoma deflected up (25 degrees from neutral), opisthosoma deflected down (25 degrees from neutral), and neutral opisthosoma with shell facing perpendicular to the flow. FLUENT reports the resultant force and moment due to Pressure and Viscous forces in addition to snapshot images of flow representation. Each orientation was simulated at 5 flow speeds (0.5, 1, 1.3, 10, 25m/s) to represent the range of flow speeds planned for empirical water channel testing (.5, 1, 1.3m/s), heightened seas states (10m/s), as well as maximum values from measured environmental conditions. Lift, drag, and pitching moment were calculated for each simulation. Flow lines, velocity profiles, and pressure distributions were also calculated for each case.

Based on the data collected, two variations of the baseline 3D computer model shells were created for simulation and empirical testing.

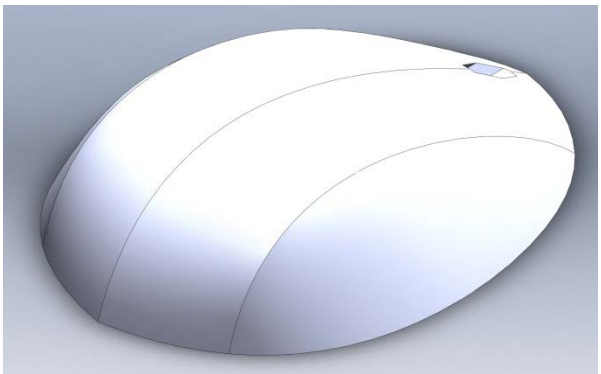

Figure 9: 3D Model Smooth

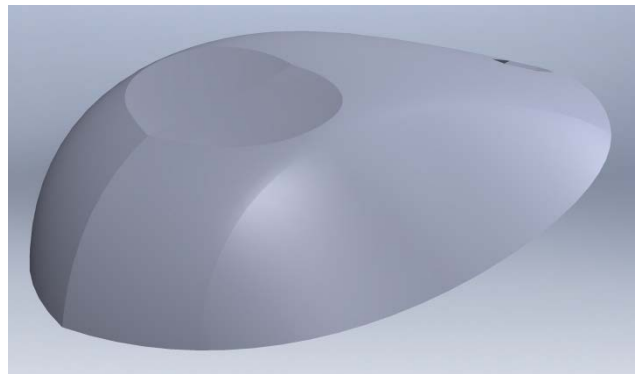

Figure 10: 3D Model Indented Top

The first design (figure 9) was modeled with a smooth profile and without the discrete joint between the anterior and posterior sections. The design intended to minimize drag by making the shell smooth and eliminating any surface features which could cause unnecessary flow disruption. The smooth shell was used as a base from which to generate the other modified designs. This allowed easy comparison of the results with other test cases. The design, as expected, resulted in decreased drag over other experimental designs for flows in all tested orientations. Removing the hinge improves the streamline profile of the shell design. The baseline design is not streamlined; therefore drag on the body is expected to be significantly higher than any of the other streamline designs.

The second design (figure 10) was modeled with an indentation at the apex of the shell intended to induce a turbulent boundary layer earlier in the flow. The indentation is placed so that the leading edge of the depression lies near the lowest pressure region observed in the biological shell tests. The primary intent of the indented design was to add a spoiler effect to reduce the lift generated by the shell in states of increased flow velocity. Fluent simulation was run to find flow lines for the Indented Top.

Copyright Applied Research Associates, Inc., 2014

The third design was modeled after the QinetiQ C-Talon robotic crawler. The C-Talon represents the industry standard for marine treaded crawlers. The model was scaled to have a frontal area and total volume similar to the smooth shell to make an adequate comparison. For simplicity, the model was given no ground clearance to remove affects of flow underneath the vehicle. Fluent simulation was run to find Flow lines for the C-Talon.

Following the CFD analyses the three most promising 3D computer models were rendered in ABS plastic using a MakerGear 2M 3D printer (figures 11, 12, 13).

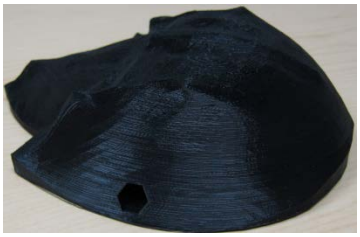

Figure 11: Baseline

Figure 12: Smooth

Figure 13: Indented Top

The three modeled hull designs were subjected to empirical testing at Scripps Institute of Oceanography (SIO) in the Hydraulics Laboratory using the Stratified Flow Channel. The flow channel test plan can be found in Appendix A. The Channel is 30m long, 1.1m wide and 1.1m deep. A computer system automatically controls flow velocity uniformly, which is variable from zero to 1.3 m/s.

The SIO Stratified Flow Channel is outfitted with a custom test fixture (figure 14) for analyzing the drag and lift on various 3D models. The fixture is a metal frame suspended above the channel. It is a three dimensional four bar linkage, which is mounted on eight flexural pivot points; four above and four below. This design is used for its extreme sensitivity to external forces and to remove any frictional forces that would interfere with the accuracy of the collected data. Additionally, the linkage and pivot points allow the frame the keep a test sample vertical during variations in the fluid flow. The frame is instrumented with individual load cells to measure drag and lift forces induced by the flow velocity on a shape within the flow channel.

Copyright Applied Research Associates, Inc., 2014

Figure 14: Flow Channel Test Fixture

Figure 15: Experimental Setup

A rigid beam (figure 15), with an airfoil cross section, is mounted to the bottom of the fixture and protrudes downward, in the direction of gravity, into the center of the flow channel in both the Y and Z plane (width and depth). The three hull shapes were tested in the center to avoid any velocity differences across the channel. The hull shapes, during individual tests, mount to the rigid beam with a custom, low drag, bracket (figure 16). The bracket was machined to have an airfoil profile. The three hull designs were mounted with their side view facing up (figure 17). This was done to ensure rigid mounting of the 3D shapes and does not affect the resulting data. Testing in the Stratified Flow Channel for drag and lift was conducted on three shapes at three flow velocities for a total of nine experiments. A typical test will last for 100 seconds. A computer is used to collect load-cell data for lift and drag from each test run at a sampling rate of 100Hz.

Copyright Applied Research Associates, Inc., 2014

Figure 16: Model attached to bracket

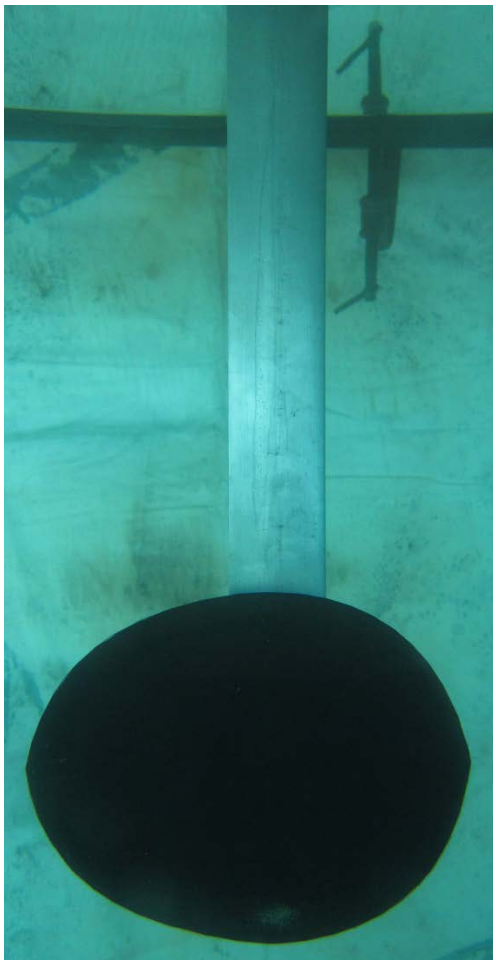

Figure 17: Testing configuration

Archimedes Screw Design

The Archimedes screw drive design research was also initiated with background literature research. The most salient research into screw drive propulsion discovered was a paper by Dr. B.N. Cole entitled "Inquiry into Amphibious Screw Traction," 1961. Cole's research used empirical testing to determine the optimal geometry (figure 18) for screws to be used as propulsion for a troop transport vehicle. Two screws being oppositely handed and contra-rotating were used to propel the machine either aground or afloat. Cole's research concluded many design features and lessons learned for future integration efforts. He determined that a helix angle of approximately 30 degrees was the best "base all around" angle for both propulsion in an air/water interface and used as a driving force on sand. A value of 0.375 for the ratio of helix blade height to drum diameter represents a good compromise between the conflicting demands of propulsive surface and general robustness of construction. This ratio combined a reasonable proportion of 'propulsive' cross-section with good mechanical strength. Both driving torque and thrust were considerably greater for the longer rotors, which relates directly to the greater total number of helix convolutions. Additionally the rotors should rotate oppositely in directions 'inward at the top' for normal forward travel. Lastly, he validated that the center of

Copyright Applied Research Associates, Inc., 2014

gravity should lie slightly aft of the midlength point of the rotors so as to prevent any possible tendency for the rotors to nose downwards into the sand bed[12]. This research was used to gain a better understanding of geometrical design considerations that would influence the mobility of a robotic system on the aquatic floor in the near shore environment.

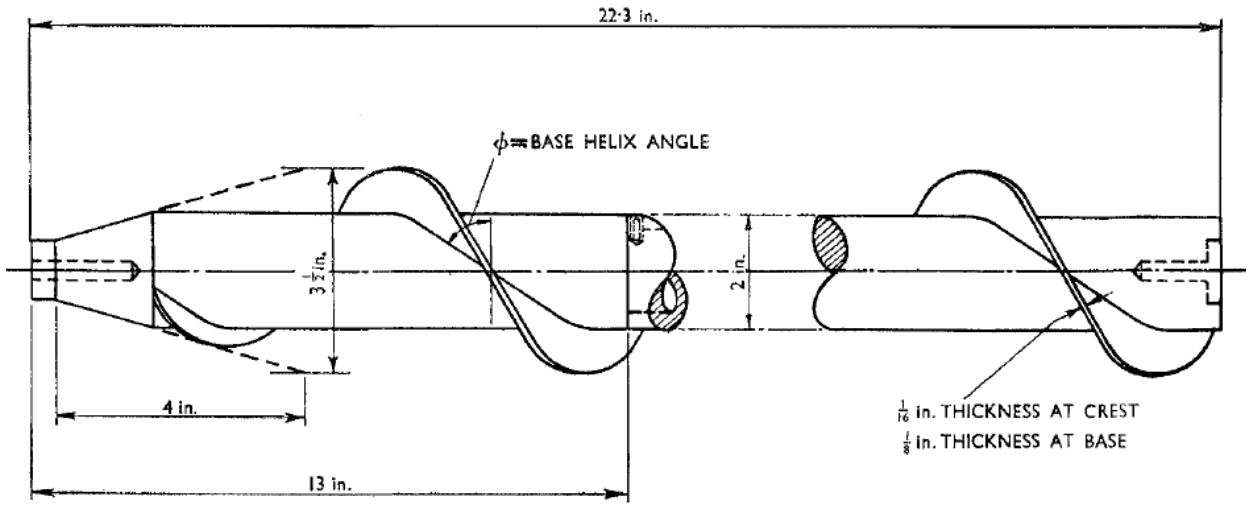

Figure 18: Single-start Archimedes Screw[12]

Some information from Cole's paper along with associated scalability factors (experiment size constraints and sensor specifications) were used to design a baseline parametric screw drive, determine the experiment set-up and scale, and define the experiment method. This lead to the design of an experimental setup for testing proposed screw designs composed of a platform for driving the screws and a channel that could be filled with different mediums (figure 19).

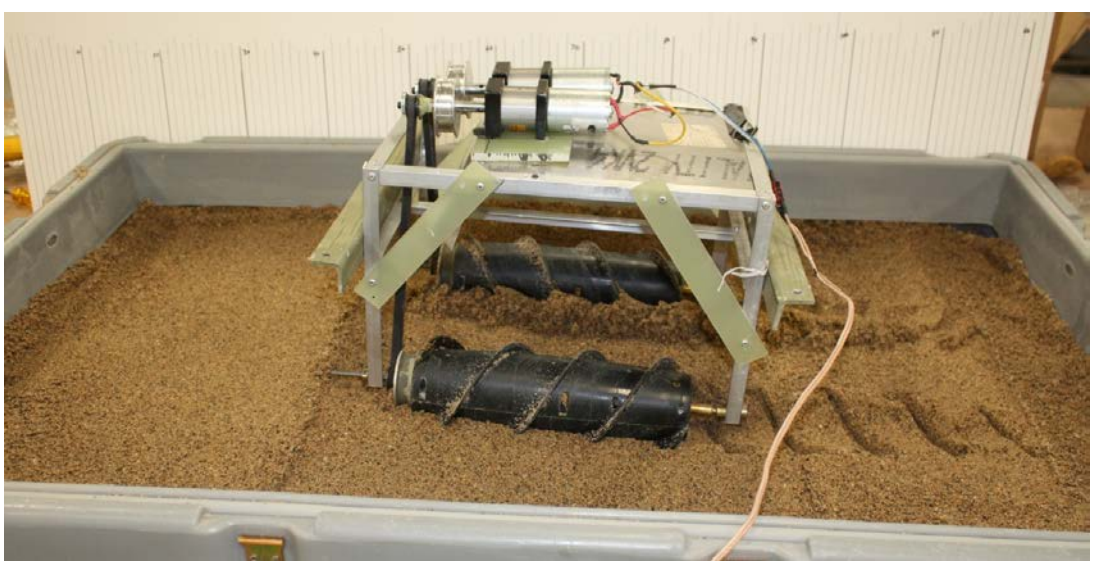

Figure 19: Experimental Test Bed and Platform

Copyright Applied Research Associates, Inc., 2014

The test bed was designed to support and rotate the test screws at a variety of speeds to determine efficiency, speed of advance, and towing capacity. This test setup enabled data to be collected for each screw design in several different mediums; water, sand, and pebbles. Selection of the mediums used was based on availability against a measured standard and overall size of the test bed. The formal test plan can be found for reference in Appendix B.

The following parameters were varied for testing:

- Medium: Wet sand, dry sand, pebbles, silt, standing water on sand
- Voltage
- Weight of test carriage

The following stimuli were measured in each test case:

- Screw drive carriage displacement to determine speed of advance, acceleration, and slippage
- Current draw to determine power use
- Qualitative observation of screw effectiveness and slippage

The tests were recorded on video against a measurement grid to determine velocities and displacements. Each experimental setup was tested ten times to get a good estimate of velocity.

Lastly, the screws were tested in an actual shore environment to gather qualitative data on system effectiveness and for better understand of challenges related to a real-world environment.

One of the key drivers behind the experimental setup was the design of the Archimedes screw drive test samples. The goal of the design was to create a screw that would optimize the screw's performance in generating forward motion on solid mediums. The first step was to design a parametric screw (figure 20) in SolidWorks with the following variable parameters: barrel length and diameter, flange height and pitch, front end taper and number of starts (quantity of flanges). These geometries were based upon conclusions from Dr. Cole's paper as a starting point.

Figure 20: Parametric Design

Copyright Applied Research Associates, Inc., 2014

Results and Discussion

Biomimetic Hull Design: Fluent CFD Modeling

Flow lines, velocity profiles, and pressure distributions for the baseline shell were calculated for each flow velocity case (figures 21, 22, 23). Further results from CFD analysis of the baseline model are available in Appendix C, figures 43 and 44.

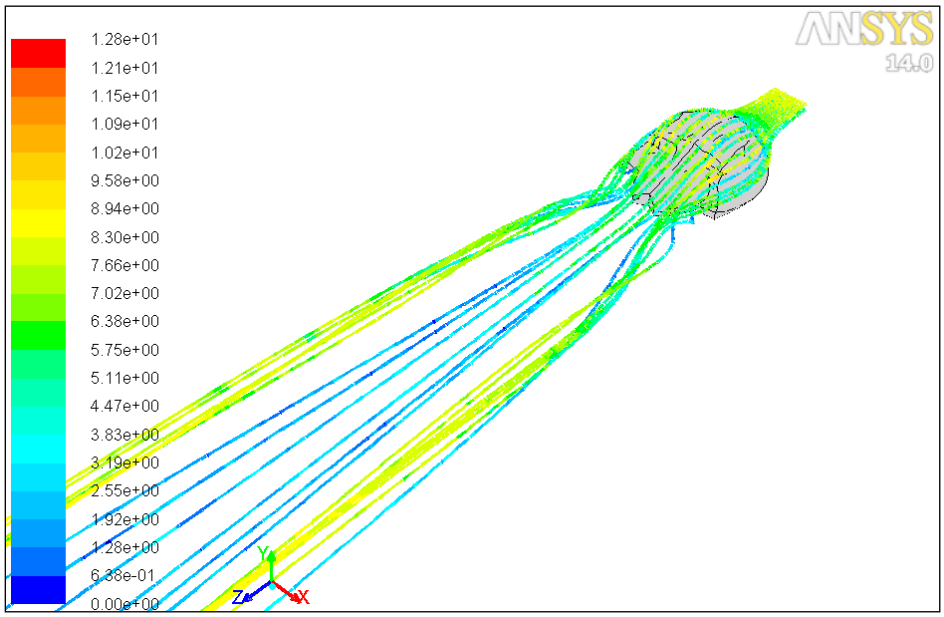

Figure 21: Flow Pathlines for Neutral Opisthosoma at 10m/s

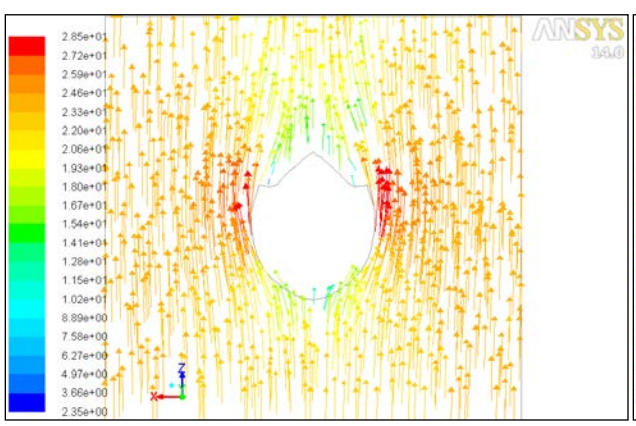

Figure 22: Velocity Vectors at 25m/s

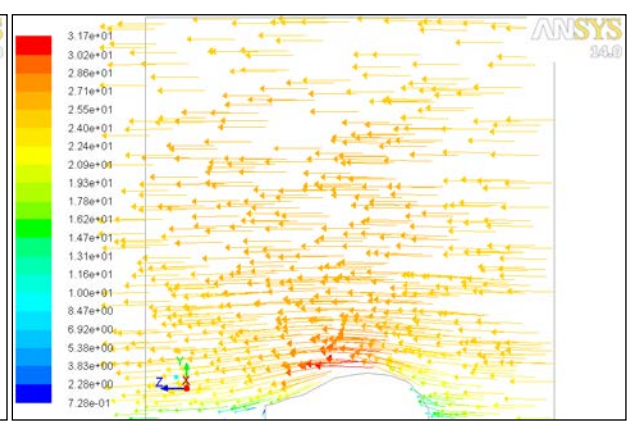

Figure 23: Velocity Vectors at 25m/s

Copyright Applied Research Associates, Inc., 2014

In all cases analyzed for the baseline 3D computer model, lift was calculated to be higher than drag. Pressure effects were greater than viscous effects. Based on the velocity profiles it is apparent that several features of the horseshoe crab shell induce turbulent flow changing the pressure distribution on the shell. The lowest pressure regions were on top of the anterior portion of the shell or prosoma, concentrated around the eyes and central ridges. This seemed to indicate that the small ridges on the horseshoe crab shell act as vortex generators and induce a turbulent boundary layer. This type of vortex generation reduces flow separation and drag.

In most cases flow separation occurred at the joint between the prosoma and opisthosoma. This flow separation and the resulting wake were judged to be the largest driver of drag. In comparison to a neutral opisthosoma, drag effects are worsened when the hinge is either flexed up or down. When flexed up, the tail increases flow separation increasing drag. When flexed down, the overall streamlined length is reduced and flow separation is again negatively impacted. The hinge and other features of the shell seem to increase drag with no related hydrodynamic benefits. These features are assumed to provide benefits to the horseshoe crab not related to hydrodynamics and thus were not considered of interest in this study.

CFD results of the flow lines for the smooth shell are displayed in figures 24 and 25.

Flow lines for the Indented Top can be found in Appendix C, figures 45 and 46. Flow lines for the C-Talon can be found in Appendix C, figures 47 and 48.

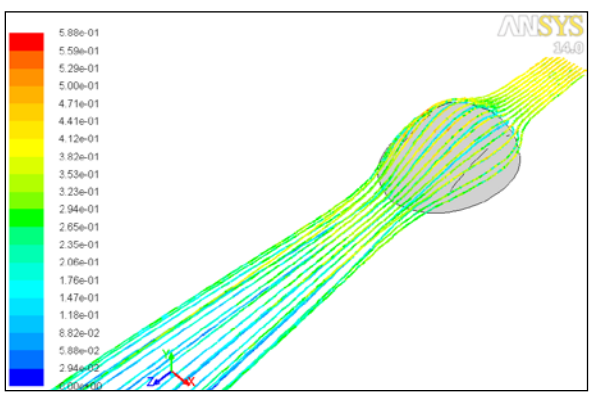

Figure 24: Flow Pathlines for Smooth Shell

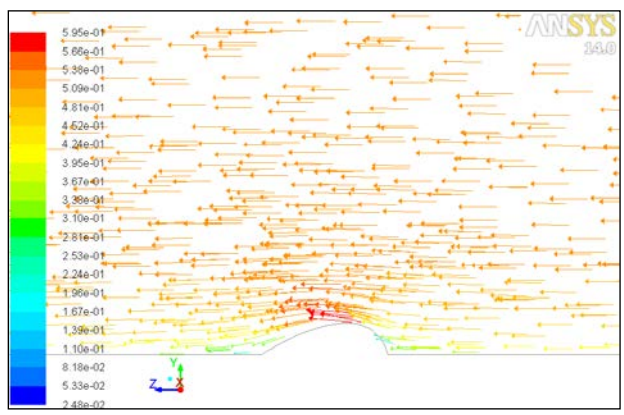

Figure 25: Velocity Vectors for Smooth Shell

For the biological shell, turbulence initiates at the eyes (1/3 of the shell length from the nose) and is worsened by the opisthosomal hinge (2/3 of the shell length). The simplified and improved designs have features that intended to decrease the overall lift without significantly increasing drag. Numerous designs were considered to meet this purpose; preference was given to designs which stayed closer to the optimal shell shape and did not require large protrusions. These new designs were compared with the baseline biological shell for hydrodynamic efficiency. The baseline model was tested to see if there was a significant impact to drag reduction from the deflection of the hinged opisthosoma. This was deemed to not reduce drag, as is evident in figure

Copyright Applied Research Associates, Inc., 2014

26. The indented top design was expected to outperform the biological shell and the smooth shell in both drag and lift. Theoretically, its design conception was sound, but FLUENT modeling proved otherwise. The indentation resulted in higher drag (figure 26) and similar lift (figure 27) in comparison to the smooth shell. Appendix C contains additional results from CFD analysis; drag in figure 49, lift in figures 50 and 51, and moment in figures 52 and 53.

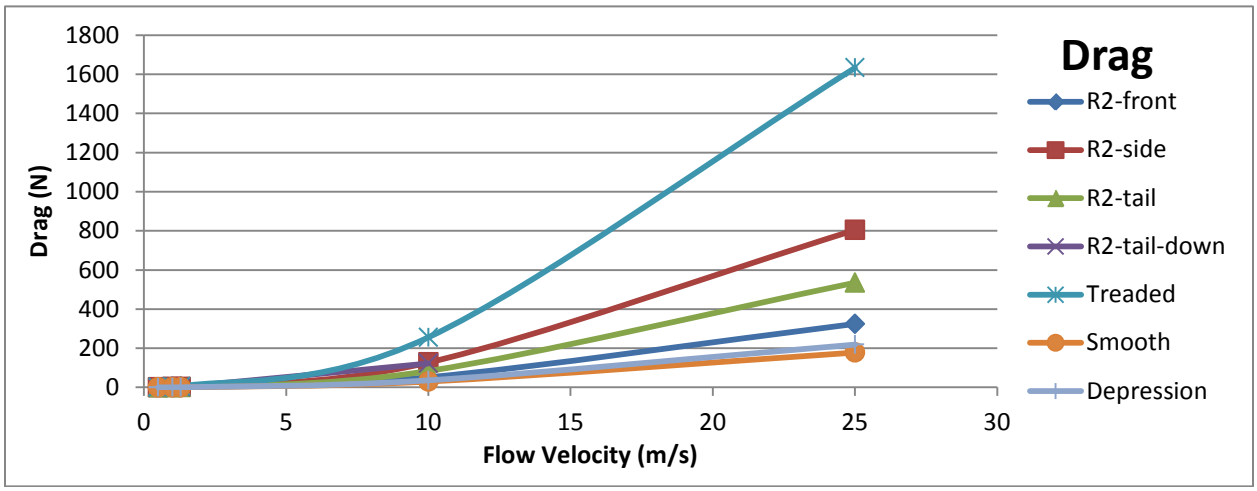

Figure 26: Drag (N) for Four Simulated Models at Five Flow Velocities

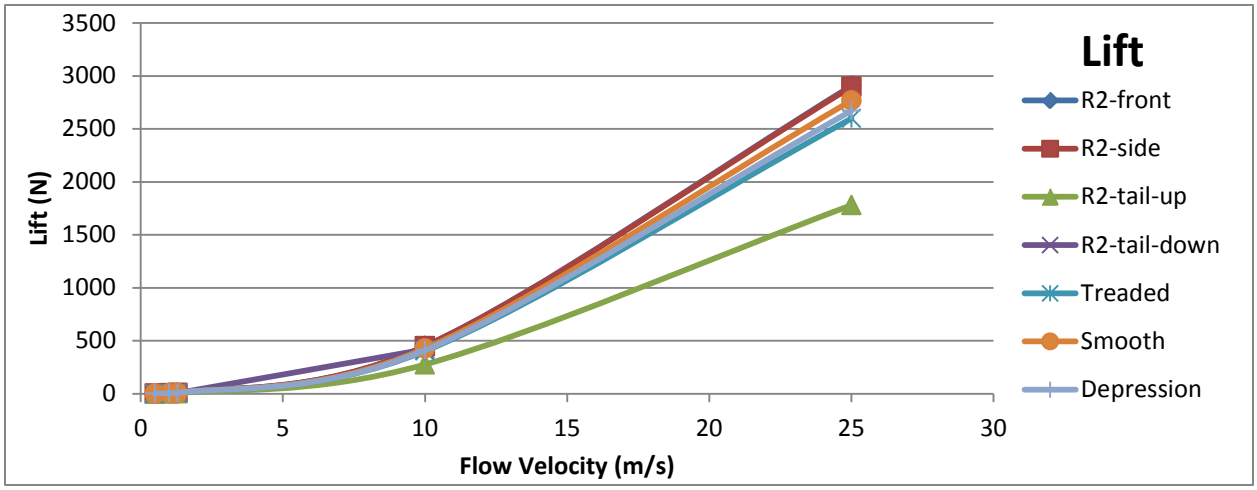

Figure 27: Lift (N) for Four Simulated Models at Five Flow Velocities

Biomimetic Hull Design: Flow Channel Testing

Testing was conducted at the SIO Stratified Flow Channel (HLab) to compare our previous Fluent CFD analysis with empirical results. This was conducted to give further confidence to our CFD results and aid in the selection of an ideal hull shape for follow-on design work. A total of nine tests were conducted on three hull shapes at three flow velocities. Data was collected for

Copyright Applied Research Associates, Inc., 2014

drag and lift each run and is available in Table 1. Table 1 directly compares the results from fluid testing at the HLab with the Fluent results. The table also displays the percent difference between the HLab and Fluent results for the same hull shape and flow velocity. There is good correlation between both results with only a few case of a difference over 20 percent. Data for comparison of lift and drag from Fluent analysis and HLab testing is plotted in figures 28 and 29. The figures reaffirm the similarities in the data and give confidence to the Fluent results.

Table 1: Comparison of Fluent CFD and Flow Channel Test of Lift and Drag

Model	Velocity	HLab	Fluent	Difference	Hlab	Fluent	Difference
	(m/s)	Mean Lift (N)	Total Lift (N)	%	Mean Drag (N)	Total Drag (N)	%
BASELINE	0.5	0.829	0.828	0.075	0.551	0.595	8.078
BASELINE	1	2.897	3.549	22.494	2.265	2.427	7.159
BASELINE	1.3	6.256	6.114	2.331	3.666	4.125	12.507
SMOOTH	0.5	0.606	0.828	36.529	0.118	0.102	15.401
SMOOTH	1	3.372	3.607	6.974	0.365	0.369	1.074
SMOOTH	1.3	6.742	6.260	7.706	0.578	0.603	4.298
DEPRESSION	0.5	1.068	0.788	35.493	0.094	0.114	21.914
DEPRESSION	1	3.179	3.443	8.315	0.509	0.422	20.590
DEPRESSION	1.3	5.727	5.983	4.477	0.591	0.695	17.503

Copyright Applied Research Associates, Inc., 2014

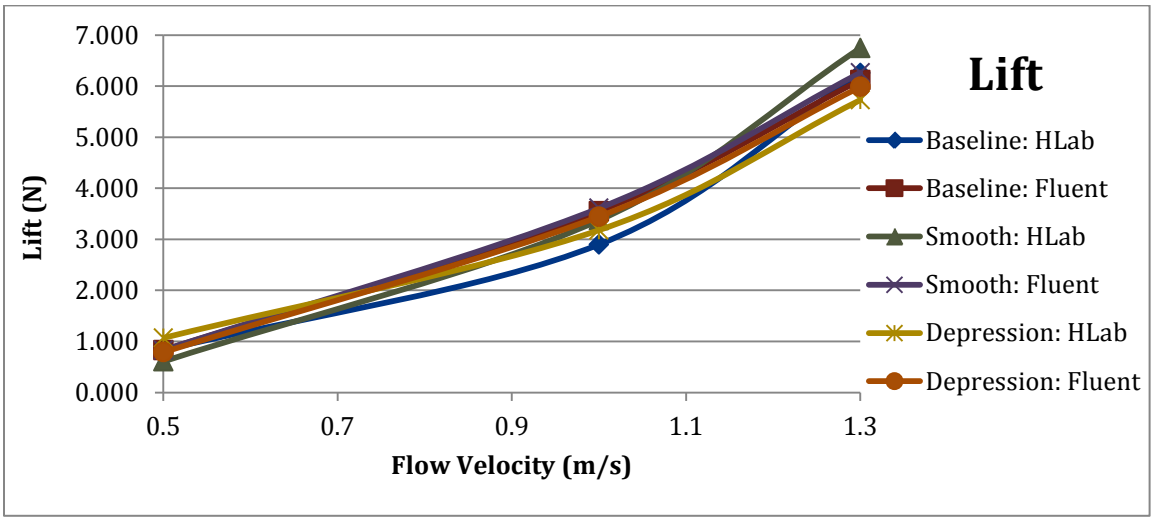

Figure 28: Lift (N) for three models at three flow velocities

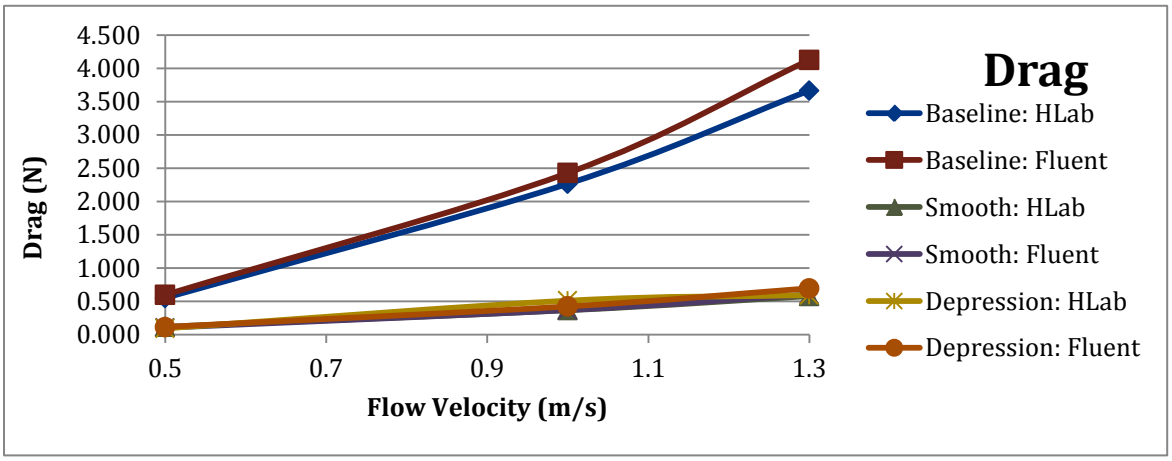

Figure 29: Drag (N) for three models at three flow velocities

Some differences in the data are expected between CFD modeling and empirical testing. These primarily result from issues relating to the mechanical equipment used in flow testing. There are slight mechanical variances, such as pump speed, flow velocity, and water turbulence, between tests in the Stratified Flow Channel. The 3D printed parts have a different surface roughness, due to the limitations of 3D printers, than the computer modeled parts used by Fluent. In Fluent testing, there was no flow modeled over the bottom of the hull in the assumption that the shell was flat on the seafloor. Whereas, in the fluid channel, flow past over the entire 3D shape. This is a limited impact because the flat bottom, normal to the flow, does not have a pressure force, which is the dominant contributor to drag and lift. Lastly, the Fluent testing was conducted in saltwater versus the SIO testing that was conducted in freshwater. This is a simple adjustment in

Copyright Applied Research Associates, Inc., 2014

the calculations, but leaves room for potential error. These individual differences are not significant alone or even all together.

The fluid testing confirms that both the smooth and depressed shapes have lower drag at the same respective fluid velocity than the baseline shape. Additionally, the testing confirms that the smooth shape has the lowest drag (figure 28), but average lift (figure 29). The similarities in the test data give strong confidence to the Fluent results, specifically in the tested region of flow velocities, and to a lesser extent in higher velocity flow cases. The coefficients of drag and lift, Appendix D figures 54 and 55, also show a strong similarity and give further confidence to the Fluent results. These are dimensionless values, used for calculating drag and lift forces in future hull shapes that are scaled in size.

Archimedes Screw Design and Testing

Extensive testing was done on screws with the parameters found in Table 2 and with corresponding images in figure 30.

Table 2: Screw Parameters for Four Designs

Screw	Barrel diameter	Flange height	Width between rotations (Pitch)	Flange thickness	Flange type
A	61mm	14.5mm	62mm	2.2mm	Smooth
B	61mm	13.8mm	42mm	2.0mm	Smooth
C	61mm	9.25mm	63mm	2.65mm	Notched
D	61mm	8mm	63mm	1.85mm	Smooth

Figure 30: Four Screws: A, B, C, and D (from left to right)

Copyright Applied Research Associates, Inc., 2014

The following sections detail the results of each test with the screws in figure 30 on the given mediums.

Wet sand

The screws listed above were tested on wet sand (figure 31) at two motor voltages (7.0V and 11.0V), and once with added weight. Ten tests were run of each setup to get averages. For tests where there was excessive slippage, ten tests were not always finished.

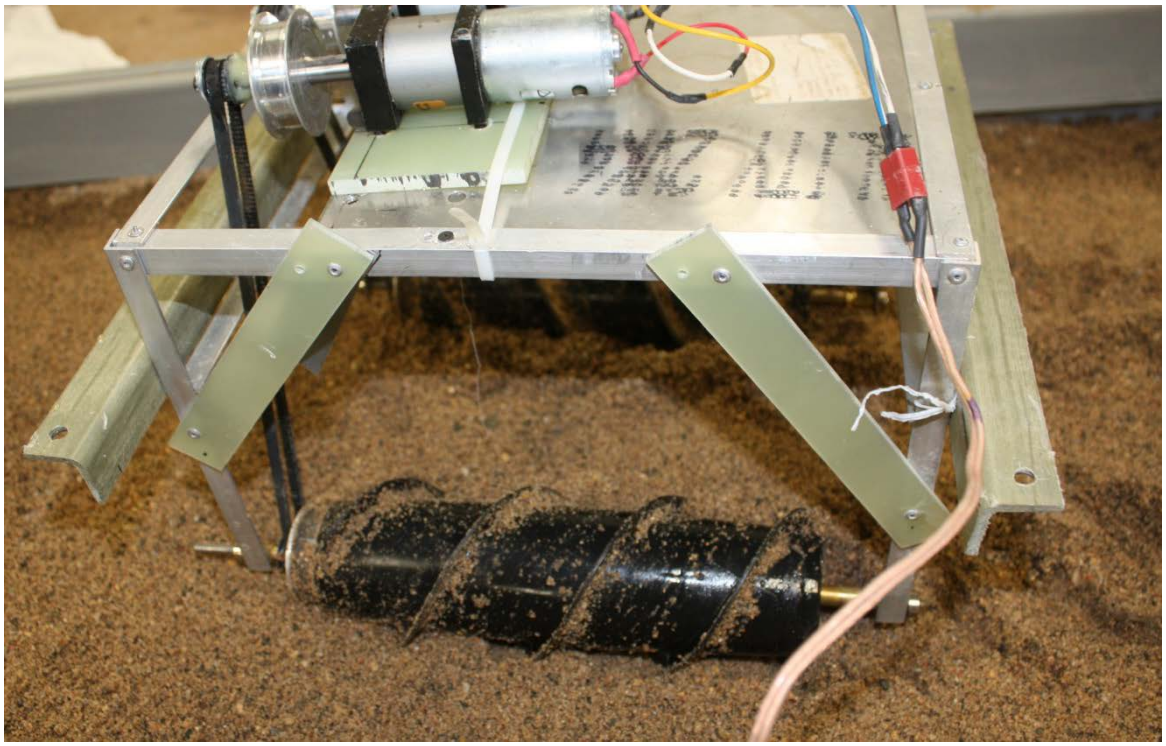

Figure 31: Screw D Tested in Wet Sand

The energy use, in units of Watt-Seconds per meter, gives a general comparison of how fast the different screws would consume battery power to cover the same distance (figure 32). The average displacement gives a general idea of how far the test platform could move before there was excessive slippage, caused when too much torque is required. The platform speeds of the different screws, for the given tests, are in figure 56 in Appendix E.

Copyright Applied Research Associates, Inc., 2014

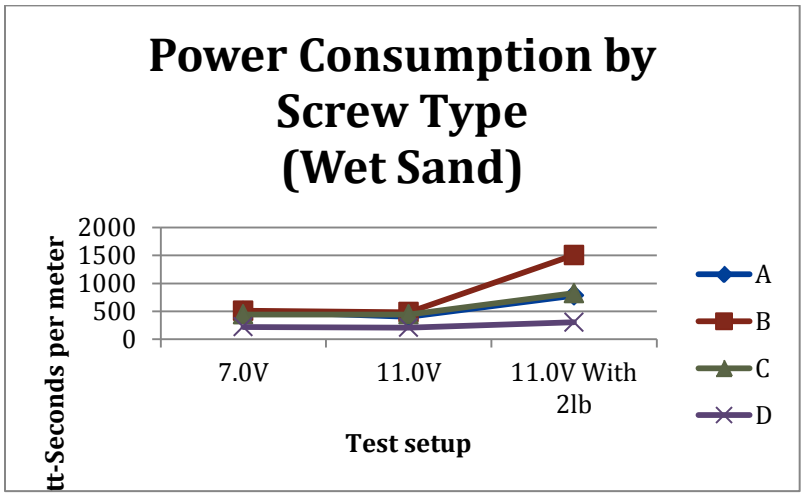

Figure 32: Power Consumption in Wet Sand

Note that for most screws increasing the speed was more energy efficient on wet sand.

In our wet sand tests, Screw D tended to require the least amount of torque and power for a given distance and was faster than other screws. Screw A was next, followed by C, then B. The full results can be found in table 5 of Appendix E.

Rock

The screws were tested on a bed of small, dry gravel (figure 33). Like the sand tests, two voltages (7.0 and 11.0V) were used, one test involved an added two pound weight to the test platform, and ten tests were attempted of each setup. The full results are shown in table 6 and figure 57 of Appendix E.

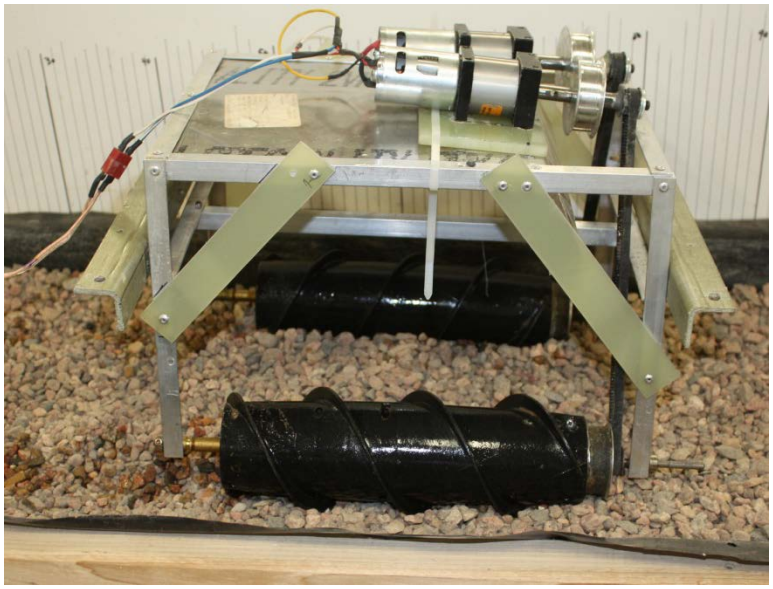

Figure 33: Screw D Tested in Rocks

Copyright Applied Research Associates, Inc., 2014

The energy usage and speed tests in rocks are shown in figure 34.

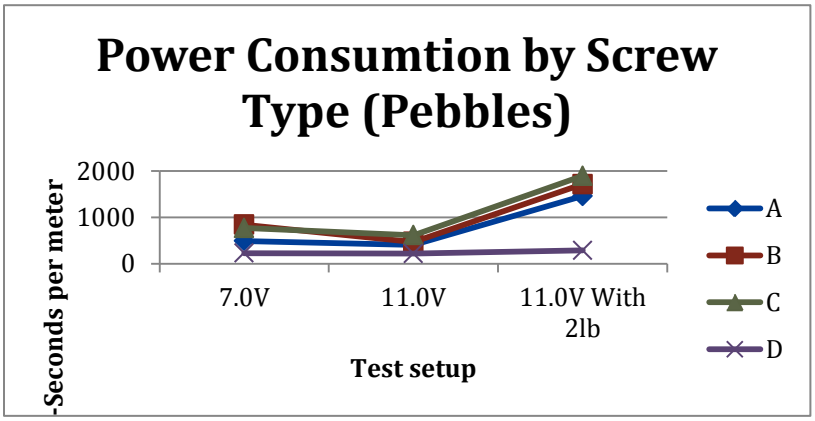

Figure 34: Power Consumption in Pebbles

Water

In order to investigate swimming capabilities of the screws in case the robot needed to navigate over or around obstacles, water testing was completed. The test platform was floated so that the motors would be out of water but the screws fully submerged (figure 35). Only one setup of each screw was run at one voltage, 10.1 V. The full results are shown in Table 7 of Appendix E.

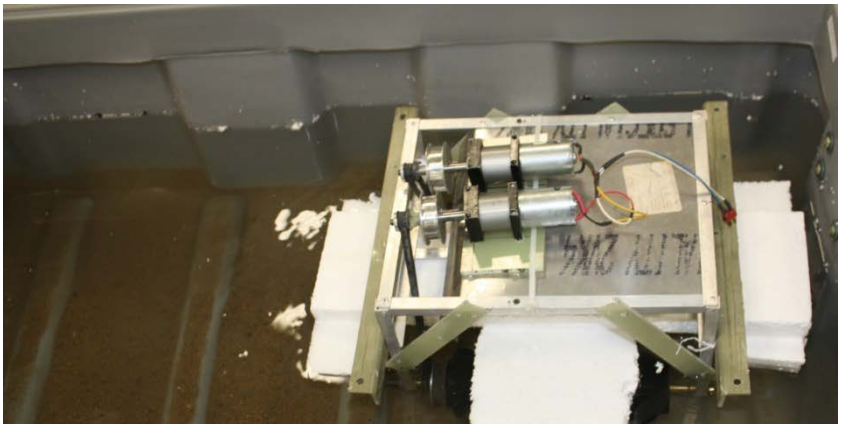

Figure 35: Water Testing

All screws worked reasonably well at propelling the test platform through water with relatively little energy. The power use and velocity of the different screws in water are visualized in the figures 36 and 37. Only one test setup was used as mentioned above.

Copyright Applied Research Associates, Inc., 2014

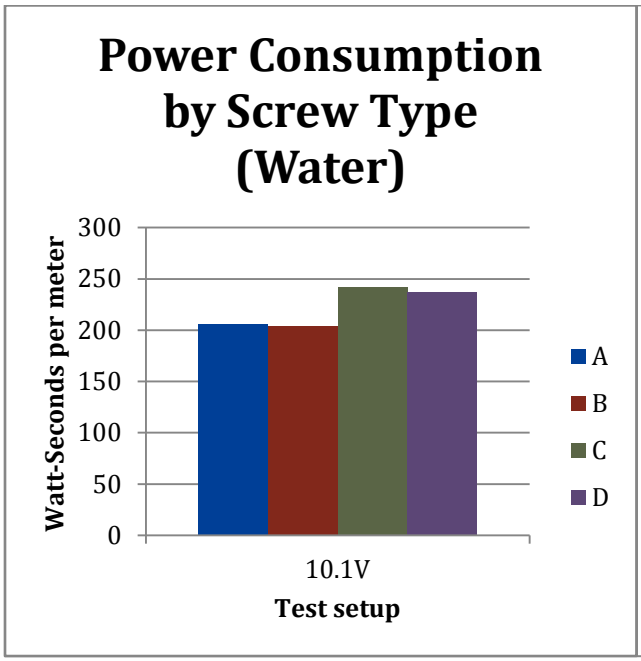

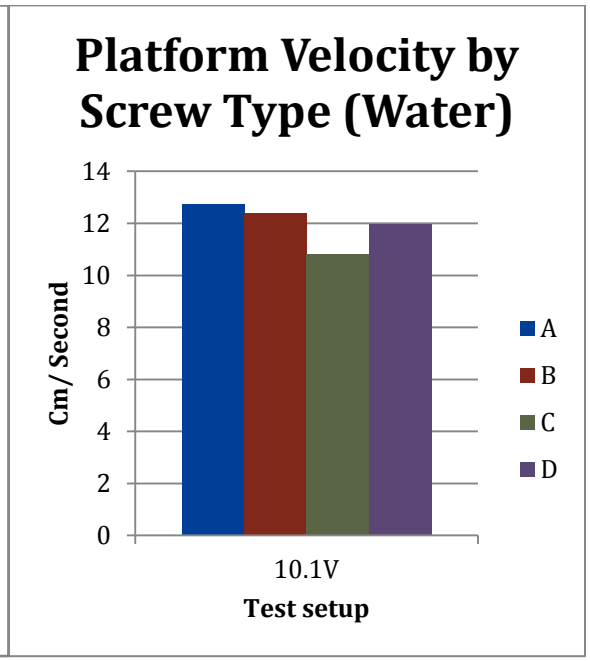

Figure 36: Power Consumption in Water *Figure 37: Platform Velocity in Water*

Because of the great variance of the screws on solid mediums, we recommend optimizing screws for land and shallow water travel since there was not much difference in speed or energy use in our water tests. Additionally, since all screws used small amounts of energy suspended in water compared to solid surfaces, if it is feasible for the application then the robot should swim whenever possible to save energy.

Dry Sand, Silt

For both dry sand and (mostly dry) silt, our test bed could not work reliably enough to collect good data. Silt especially took immense amounts of torque to move the test bed. For a real surf-zone robot, these will likely be the most difficult mediums to move through.

Skid Testing

In order to study the effects of the robot platform on screw effectiveness a set of skids were added on the underside of the test platform. The height of the skids could be adjusted to study the impact of useful screw depth below the bottom of the test bed. It was important to know if any portion of the screw could be recessed within the hull of a future deign or if the screws needed to be fully separate from vehicle, similar to the design in Cole's paper.

Copyright Applied Research Associates, Inc., 2014

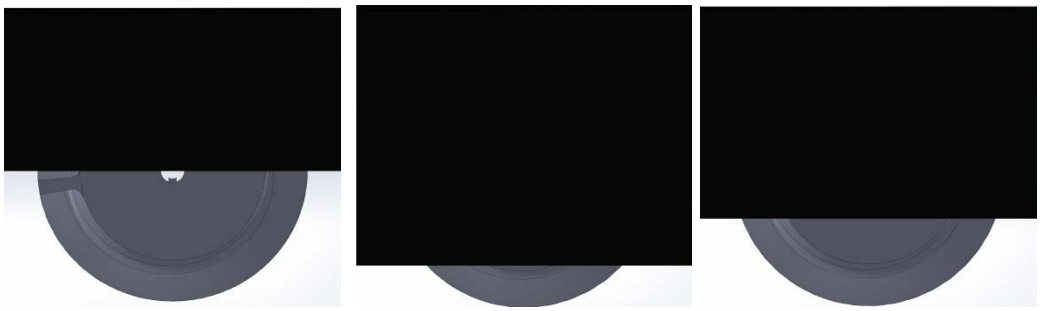

Figure 38: Three tested screw depths below test platform (1, 2, 3 from left to right)

Only one screw type was used in ski testing, screw D. Three ski heights were tested as shown in figure 38.

- 1: Bottom of skid at axis of rotation of screw
- 2: Bottom of skid at bottom of barrel diameter
- 3: Bottom of skid midpoint between bottom of barrel and axis of rotation

On wet sand, which compacts well and causes the screws to dig in only a small amount, ski heights 1 (figure 39) and 2 worked effectively, and screw height 3 did not. At height 3 the screws would dig a trough and the robot would be effectively "beached".

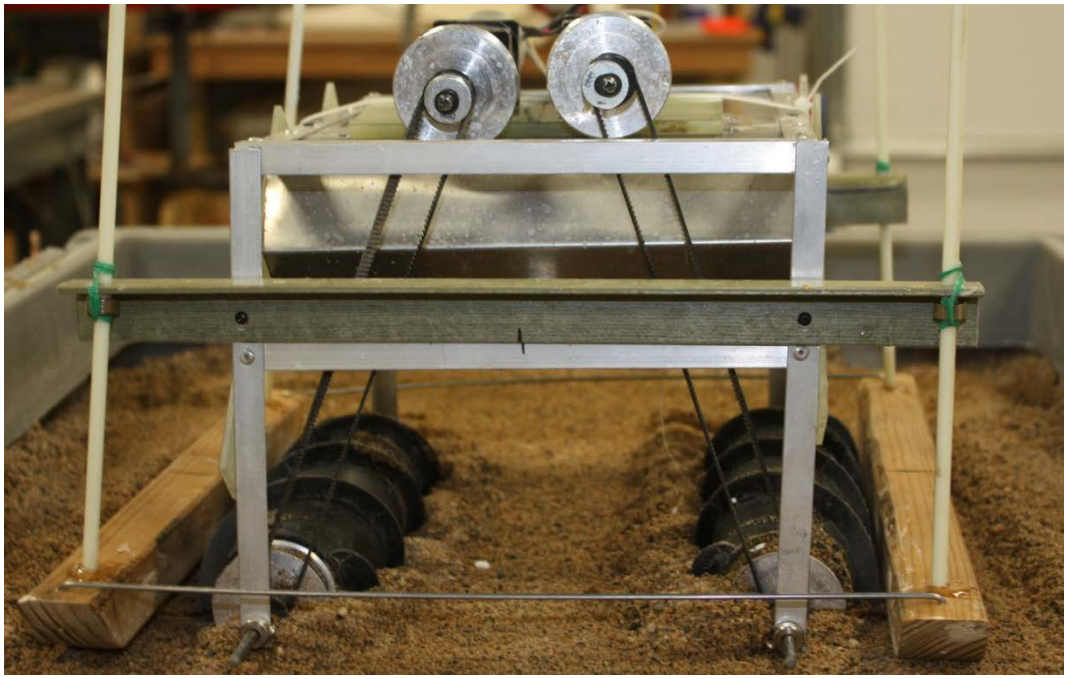

Figure 39: Skid Testing Configuration 1 (skid at axis of rotation)

Copyright Applied Research Associates, Inc., 2014

On gravel, which digs down more easily, heights 2 and 3 did not work. Height 1 worked only marginally, with the test bed moving slowly and erratically.

On a full surf-zone robot in which the screws were under the shell to prevent waves from flipping the robot, it is likely that the amount the screws are lowered under the bottom of the robot would need to be adjustable. In very shallow water or dry land the screws would be most effective fully lowered out of the body of the robot. In deeper water the screws should be recessed as much as possible, and when the robot is stuck the screws could be lowered temporarily.

Shallow Water Test

In order to better understand the dynamics of a real-world shore environment, as a final test the test platform was taken and driven in an actual lake shore (figure 40). Only screw set D was used in these tests.

Figure 40: Shallow Water Testing

The test platform was able to drive reasonably well in the shallow water on silt, but tended to angle quickly downhill because of the slope of the shore. On an actual surf-zone robot it is likely that the uphill screw would have to drive more slowly to continue driving parallel to the shore.

Driving the platform from water to land was tested, and it was found that the platform drove more easily in water than on land, which was comprised of dense, dry silt. Silt and mud would likely be the most difficult surface to drive on, because of how dense and sticky the substances are.

Copyright Applied Research Associates, Inc., 2014

Conclusions and Implications for Future Research

Biomimetic Hull Conclusions

Fluent modeling was used to compare different potential hull shapes for optimizing the design of a future VSW/SZ robot. The Limulus Polyphemus shell was used a baseline model. Two other similar shapes where modeled with improved drag reduction characteristics. The CFD modeling confirmed that the smooth shell had the lowest drag in comparison to the baseline model, the indented top, and the QinetiQ C-Talon robotic crawler.

Empirical flow testing was conducted to confirm the results of the Fluent CFD analysis. Three 3D printed hulls were tested at the same flow rates as CFD modeling for comparison. Test data showed that for the same flow velocities the baseline shape has higher drag than the smooth and indented shapes. The experiments confirm that the smooth hull had the lowest drag of any shape tested. There is also strong agreement between the data from the Fluent CFD modeling and the results of the empirical experiments. This gives high confidence in Fluent results. The coefficients of drag and lift also show a strong similarity.

All testing confirms that it is possible to design a hull shape to improve stability in the dynamic wave conditions found in the VSW/SZ. Both CFD and empirical testing agree that the smooth shell has improved drag reduction capabilities over the baseline model of the Limulus Polyphemus. The strong agreement in drag coefficient between the two testing methods proves promising for scaling of the hull size for a future design with increased payload.

Archimedes Screw Conclusions

As a result of testing, we recommend the following with regard to Archimedes Screw Design and use:

1. The best all-around performing screw in our tests was Screw D. An up-scaled version of this screw would be the best to use, or make the best starting point.
2. The screw flange should be no deeper than needed for reliable traction. Deep flanges immensely increase torque required to move the vehicle.
3. The screws should be as smooth as possible to prevent mud and silt sticking to the screws and to minimize the amount of unnecessary friction when turning the screw. Polished steel or aluminum, for instance, would work well.
4. Any of the screws we tested worked well for swimming while the vehicle was suspended in water. We recommend the screw be optimized for movement on ground instead, and assume it will work well “swimming” as well.
5. Using the screws for propulsion while suspended in water, or “swimming”, used small amounts of power and worked well. Depending on application and ocean currents, it may be better to swim as opposed to “crawl” when the water is deep enough.
6. In instances where the seafloor is not flat the screws will have to turn at different rates to keep the robot going straight. Good inertial navigation or similar will be needed to efficiently keep the robot moving in a straight line

Copyright Applied Research Associates, Inc., 2014

7. Depending on operating needs, the most difficult environment for the Archimedes screw is above-water silt and mud. Avoiding these areas if possible would be recommended, or if needed to be covered then expect high energy usage for the area covered.
8. The ski tests showed that if the screws are completely under the robot body the robot can "beach" in loose mediums. If the screws could be raised and lowered, then the screws could be lowered on dry land and retracted somewhat in water so that the bottom of the robot is as close to the sea floor as possible to prevent flipping.

Overall Conclusions and Next Steps

The research and testing conducted has demonstrated the ability for a robot to operate in the VSW/SZ. A shell was optimized to reduce drag and lift and aide in tractive potential. An ideal Archimedes screw drive was determined and is sufficient to be used across different mediums; such as sand, water, and gravel. These results are can influence future design efforts.

Further analysis needs to be conducted to determine what the maximum flow vectors for which the biomimetic hull can remain effective and what are the resultant forces from those maximum flow vectors? Additionally, a flow channel capable of testing upwards of 10m/s or higher would additionally aid in the analysis of the survivability of a future design.

A potential future design is depicted in figures 41 and 42. The vehicle has separate housings for individual subsystems to be replaced for maintenance. A motor housing to run the Archimedes screw is mounted in the forward section. Centered just aft of the motor housing is a swappable and rechargeable battery housing. Mounted atop the lower housings are three electronics pressure vessels. They are separated to allow access to certain electrical components without opening unnecessary seals on working components. Additionally, they geometrically nest efficiently under the shell of the housing. The Archimedes drives are spaced as wide as possible to give the vehicle a large base of support and to limit a toppling moment.

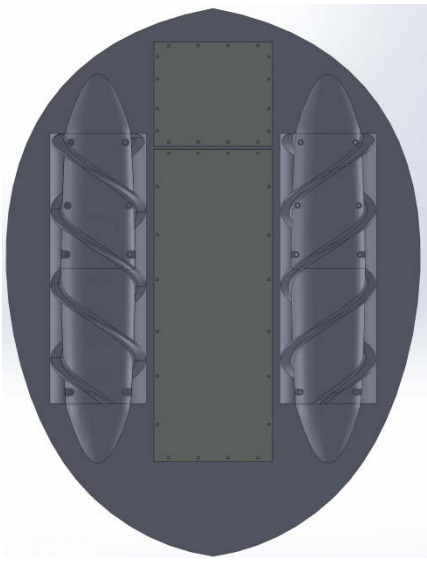

Figure 41: Design bottom view

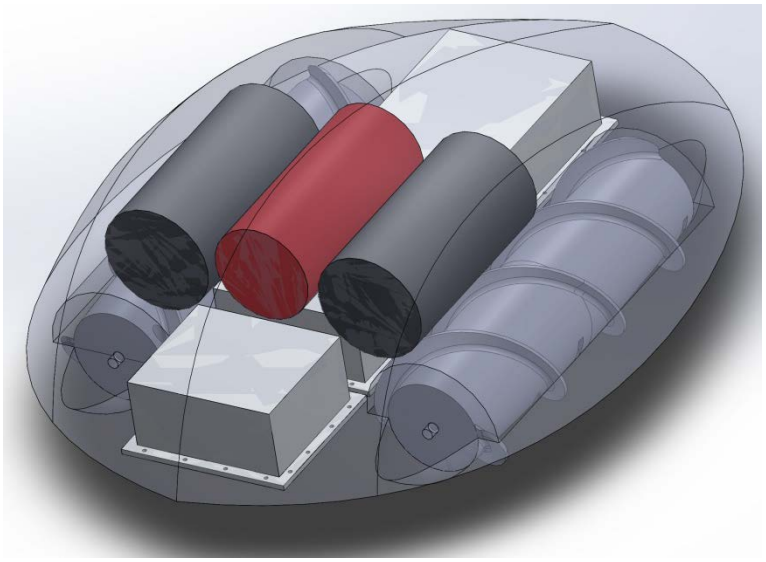

Figure 42: Design front ISO view

Copyright Applied Research Associates, Inc., 2014

Potential follow-on efforts will address the remaining subsystems in the design space of the robot including: Autonomous Navigation Hardware/Software, Communications Hardware/Software, Payload/Sensor Integration, and Power/Motor Systems. Based on the results of the after-market study ARA contends that a majority of the robotic system components can be fulfilled using COTS or near-COTS solutions as seen in table 4. Additionally, steps will be taken, in regard to platform development, to design a vehicle to grow in complexity. That is, the vehicle may initially function as a remotely operated vehicle (ROV) for proof of concept testing and transition into an autonomous vehicle (AUV). Following the construction of the prototype it will then be tested in local environment and optimized for applicable employment concept, whether that be munitions detection or use as a platform to further study the near shore environment.

Table 3: Robotic Sub-system Components from COTS Manufacturers

Manufacturer	Technology	Description
Bluefin Robotics	Subsea Battery	Hi capacity storage battery for AUV applications. Self-contained and fully waterproof.
Kairos Autonomi	Pronto 4 Agnostic Autonomy (Software)	A proven integrated autonomy package. The software can be used for high level control.
Tecnadyne	Thrusters and Rotory Actuators	Waterproof thrusters and motors for marine applications.
Teledyne Benthos	Acoustic Modem	Modems for navigation and data uplink.
IXSEA	GAPS	Underwater positioning system, integrates inertial navigation, GPS, and acoustic positioning.

Copyright Applied Research Associates, Inc., 2014

Literature Cited

[1] Strategic Environmental Research and Development Program, Environmental Security Technology Certification Program, 2007. Final Report from SERDP and ESTCP Workshop on Technology Needs for the Characterization, Management, and Remediation of Military Munitions in Underwater Environments. https://serdp-estcp.org/content/download/8054/99435/version/1/file/SERDP-ESTCP-UW-Workshop.pdf

[2] Gallager, Edith L. MacMahan, Jamie. 2007. Spatial and Temporal Variability of Grain Size and Small-Scale Morphology. http://www.dtic.mil/cgi-bin/GetTRDoc?AD=ADA514925

[3] Chung, Jin S. 2005. Deep-ocean Mining Technology: Development II. The International Society of Offshore and Polar Engineers. ISBN 1-880653-65-6 (October 9-13)http://www.isope.org/publications/proceedings/ISOPE_OMS/papers/01.pdf

[4] Scalfani, Matthew. McKown, Kim. 2088. Horseshoe Crab (Limulus polyphemus) Spawning Activity Survey Protocol for the New York State Marine District. Cornell Marine Program.http://ccesuffolk.org/assets/galleries/Horseshoe-Crab-Research/HSC-SURV08-12.pdf

[5] Lotman, Rick. 2011. Deep Sea Mining With an Archimedes Screw Driven Vehicle. ASME 2011 30th International Conference on Ocean, Offshore and Artic Engineering. Volume 5. June 19.
http://scitation.aip.org/getabs/servlet/GetabsServlet?prog=normal&id=ASMECP0020110443730001300000 1&idtype=cvips&gifs=yes&ref=no

[6] Denny, M. W. 1988. Biology and the Mechanics of the Wave-Swept Environment. Princeton: Princeton University Press.

[7] Denny, M. W. and Blanchette, C. A. 2000. Hydrodynamics, shell shape, behavior and survivorship in the owl limpet Lottia gigantea. J. Exp. Biol 203, 2623–2639.

[8] Denny, M.W. 1989. A limpet shell that reduces drag: laboratory demonstration of a hydrodynamic mechanism and an exploration of its effectiveness in nature. Can J. Zool. 67:2098-2106.

[9] Denny, M.W. 2000. Limits to optimization: Fluid dynamics, adhesive strength, and the evolution of shape in limpet shells. J. Exp. Biol. 203: 2603-2622.

[10] Vosatka, ED. 1970. Observations on the Swimming, Righting, and Burrowing Movements of Young Horseshoe Crabs, Limulus Polyphemus.

[11]Dietl, J et al. 2000. Influence of Ambient Flow Around the Horseshoe Crab Limulus polyphemus on the Distribution and Orientation of Selected Epizoans.

[12] Dr. B.N. Cole entitled “Inquiry into Amphibious Screw Traction,” 1961

Copyright Applied Research Associates, Inc., 2014

Appendix A: Biomimetic Hull Test Plan

1. Introduction

1.1. Biomimetic Hull Overview

A Biomimetic hull is proposed to shroud an underwater robot capable of operating in the VSW/SZ. The hull would take advantage of fluid flow in the VSW/SZ to aid in tractive potential and stability. Therefore, the flow would assist the robot from being displaced from its intended location of operation. CFD modeling was conducted to investigate and compare different hull shapes. A biomimetic hull shape study is proposed to verify the results of our CFD modeling with empirical testing.

1.2. Purpose

The purpose of this test plan is to verify the results of our CFD modeling with empirical testing and to determine which hull shape should be utilized in future designs.

2. Test Design

2.1. General test setup

Testing will be conducted in the Stratified Flow Channel within the Hydraulics Laboratory at Scripps Institution of Oceanography (SIO), in La Jolla, California. All testing will be conducted by SIO staff as required by their testing policies and procedures. The Stratified Flow Channel is a 30m long flooded test bed that is 1.1 m wide with a water depth of 1.1 m. A computer system automatically controls flow velocity uniformly, which is variable from zero to 1.3 m/s. Another computer is used to collect load-cell data from each test run at a sampling rate of 100Hz. Three hull designs will be tested in the Stratified Flow Channel for drag and lift.

2.2. Variables

2.2.1. The following variables will be changed during setup for a test

a) Hull Design: Baseline, Smooth, Indented Top

b) Flow Velocity: 0.5, 1.0, 1.3m/s

2.2.2. During testing the following data will be collected and analyzed:

a) Drag

b) Coefficient of drag

c) Lift

d) Coefficient of lift

Copyright Applied Research Associates, Inc., 2014

2.3. Test hull description

Each biomimetic hull will be created from a parametric 3D model and fabricated via 3D printing. The three tested hulls will vary in surface shape and features. The hull designs will be described in the final report.

2.4. Test Fixture

The test fixture is a metal frame suspended above the Stratified Flow Channel. It is a three dimensional four bar linkage, which rests on four flexural pivot points. This design is used for its extreme sensitivity to external forces and to remove any frictional forces that would interfere with the accuracy of the collected data. The frame is instrumented with load cells to measure the drag and lift forces induced by the flow velocity on a shape within the flow channel. A rigid beam, with an airfoil cross section, is mounted to the bottom of the fixture and protrudes downward, in the direction of gravity, into the center of the flow channel in both the Y and Z plane (width and depth). The three hull shapes are tested in the center to avoid any velocity differences across the channel. The hull shapes, during individual tests, mount to the rigid beam with a custom, low drag, bracket.

3. Test procedures

3.1. General test procedure

The general test procedure is as follows

1. Zero Run
    a. Mount beam and bracket into test fixture
    b. Run test at initial flow velocity
    c. Collect data to measure drag and lift resulting from beam and bracket
    d. Re-run tests and collect data for each specific flow velocity
2. Test Run
    a. Mount hull shape to bracket
    b. Mount hull, beam, and bracket to test fixture
    c. Run test at initial flow velocity
    d. Collect data to measure drag and lift resulting from beam and bracket
    e. Re-run tests and collect data for each specific flow velocity
    f. Remove hull, beam, and bracket from test fixture

Copyright Applied Research Associates, Inc., 2014

g. Insert new hull and replace hull, beam, and bracket into test fixture

h. Re-run tests and collect data for each specific flow velocity and hull

3.2. Data analysis

After the tests, the logged data will be analyzed from each run. The drag and lift from the "Zero Run" will be subtracted from the data for each of the hulls and each of the velocities. The data from each test will be entered into an excel spreadsheet to calculate drag, coefficient of drag, lift, and coefficient of lift.

Copyright Applied Research Associates, Inc., 2014

Appendix B: Archimedes Screw Test Plan

1. Introduction

1.1. Archimedes Screw Overview

The Archimedes Screw Drive is a proposed system for propelling a surf-zone robot. The rotation of the screws causes the vehicle platform to move forward through a variety of mediums, both solid mediums and with the platform floating in water.

1.2. Purpose

The purpose of this test plan is to test different types of Archimedes Screws through a variety of mediums to determine the following data:

a) Which screw parameters work most effectively in different mediums

b) How the screw drive effectiveness changes across mediums

c) Learn general lessons about Archimedes screw drives in surf-zones

2. Test Design

2.1. General test setup

The general setup of the test will consist of a test rig on which the screws will be attached, and test beds in which to place the medium. The test rig will have two motors to drive the screws, which can be changed out between experiments. The test beds will be filled with a variety of mediums to learn about the different screw characteristics. The test bed will be backed by a measurement grid and the test will be video recorded, so that the video timestamp and the test grid can be used to determine speeds and accelerations of the test rig.

2.2. Variables

2.2.1. The following variables will be changed during setup for a test:

a) Screw on vehicle

b) Motor voltage- constant for a given test

c) Added weight to rig

d) Test Medium- Wet sand, dry sand, gravel, silt, water, water on sand

2.2.2. During and after the test the following data will be collected to analyze screw effectiveness:

a) Speed and acceleration from video

Copyright Applied Research Associates, Inc., 2014

b) Amp draw of motors to determine power usage (W) and energy use/efficiency (W-s/m)

c) Displacement

d) Qualitative observations of general screw effectiveness

2.3. Test screws description

Each screw will be created from a parametric 3D model and fabricated via 3D printing. The different screws can be varied in screw spacing, flange depth, barrel diameter, and flange surface shape. The final screws used will be listed in the final report.

2.4. Test rig description

The test rig has a metal frame with the screws attached on axles on the bottom and two motors on the top. Belts are used to drive the screws from the motors. Having the motors high above the screws which are belt-driven allows the test rig to be used in water without the motors getting wet. The motors are powered over a long wire by power supply. In the lake test mentioned below, a battery will be used instead of a power supply. In any test with water the power line will be fused.

2.5. Test bed description

Different test beds will be used to test the screw drive. All consist of a tray of some sort of medium. The shallowest tray will be used for dry mediums. A deeper tray will be used for shallow water. A deep container will be used for deep water ("swimming") tests. The trays will be filled with the medium needed for a given test, and after each test run the medium will be re-graded as needed. In all cases a measurement grid will be placed behind the test bed for the video analysis of the speed of the rig.

3. Test procedures

3.1. General test procedure

The general test procedure is as follows

1. Test setup

    a. Fill and level out test bed with medium for test

    b. If test involves water, wire power cable to fuse block

    c. Set power supply to voltage needed for test

    d. Attach screw being tested to test rig

    e. If needed for test parameters, add weight to rig

Copyright Applied Research Associates, Inc., 2014

   f. Set up camera looking directly at center of measurement grid

   g. Fill out test card on edge of test bed for video listing test number, voltage, added weight, and screw. Make sure card is in frame of video.

2. Start camera

3. Apply voltage and hold until test rig either:

   a. Reaches end of test bed

   b. Reaches one side of the test bed

   c. Is immobile

4. During run, note amp draw

5. After test, re-grade bed and clean medium out of drive sprockets if needed.

6. Return to step 3 to repeat test. Attempt 10 test runs of each test setup to a achieve a good average.

3.2. Auxiliary tests

Lake Test

In order to better learn how the screw drive operates in a real-world environment the test rig will also be driven in shallow water of a river or lake. Only one set of screws and voltage will be used and general notes will be taken on effectiveness of the screws and unforeseen issues that arise.

3.3. Data analysis

After the tests are run, the data will be analyzed. For each of the ten runs, the video will be cut and checked. For each run the start and stop position of the rig will be noted by using the measurement grid, and the time between the two will be determined by looking at the video frame count elapsed and dividing by the relevant frame rate. The data from each test will be entered into an excel spreadsheet, including the average amp draw noted. Using the data in the excel spreadsheet, calculations can be made for each set of runs the average amp draw, power use, speed, displacement, and power used for a fixed distance.

Copyright Applied Research Associates, Inc., 2014

Appendix C: Shell CFD Test Data

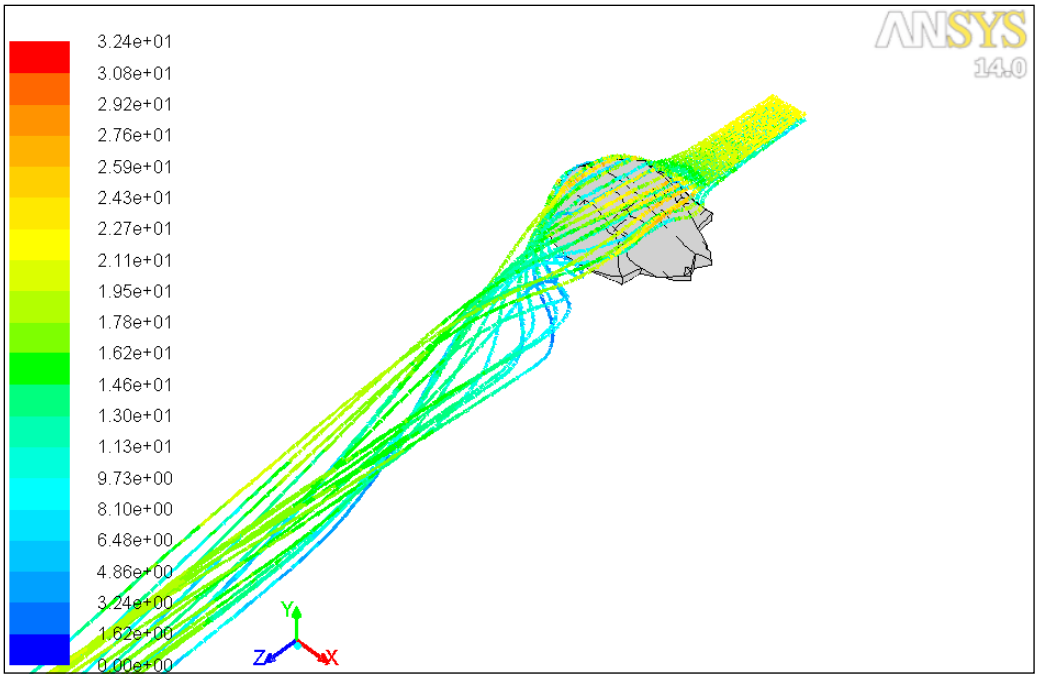

Figure 43: Flow Pathlines for Baseline Shell with Flow Perpendicular to Shell at 25m/s

Copyright Applied Research Associates, Inc., 2014

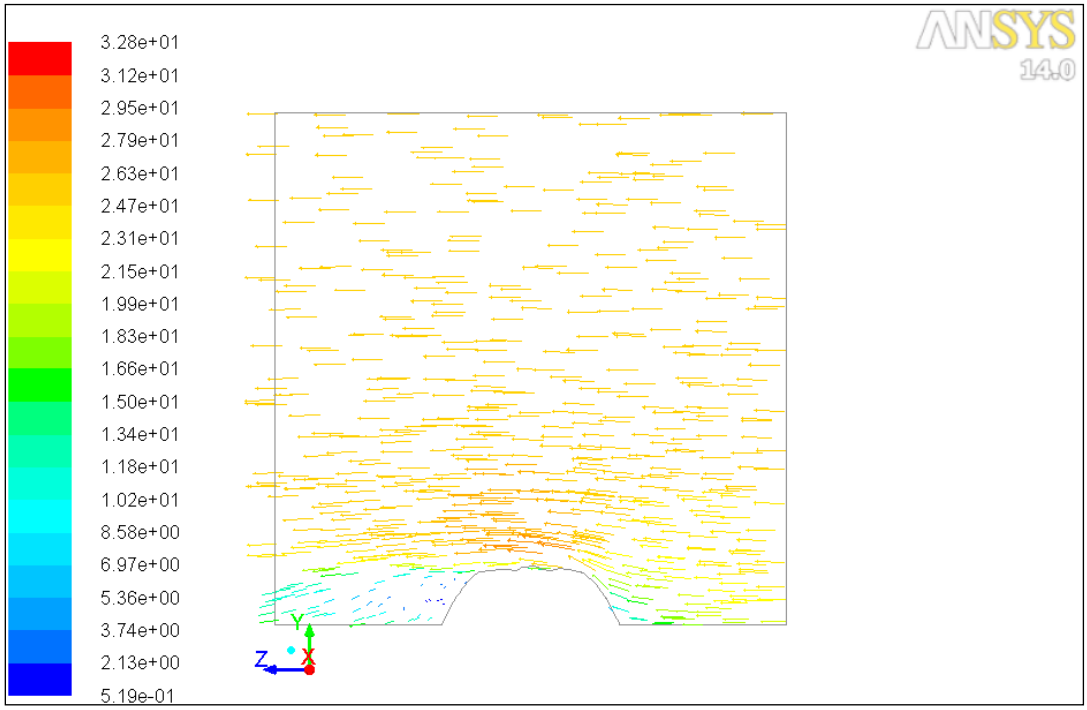

Figure 44: Velocity Vectors for Baseline Shell with Flow Perpendicular to Shell at 25m/s

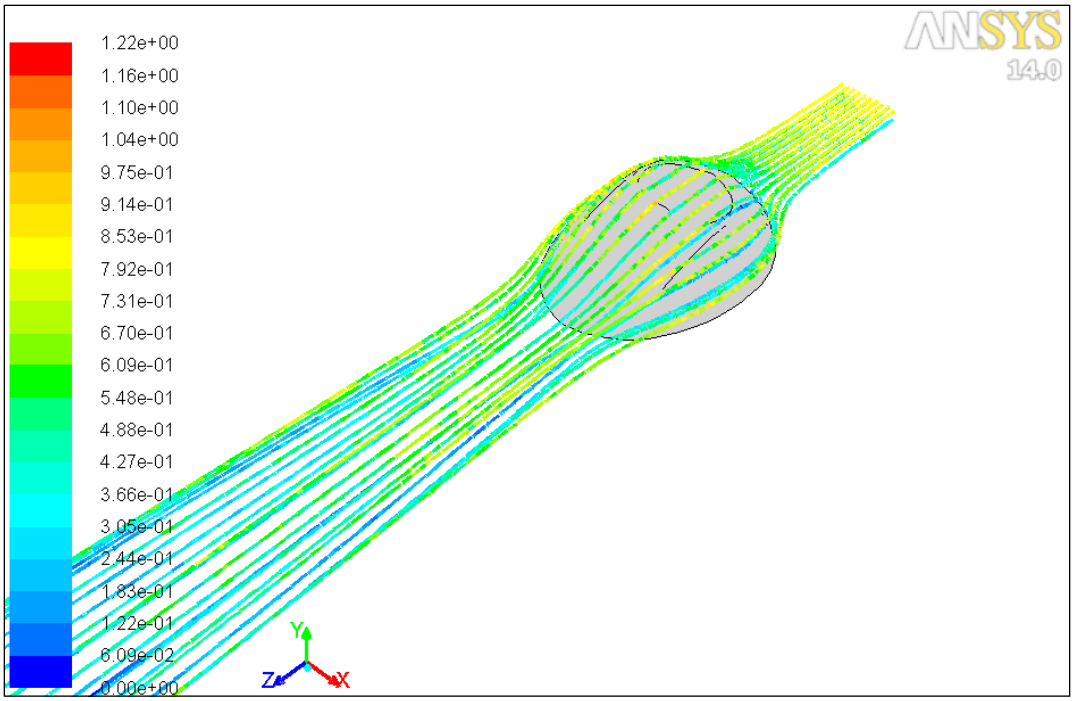

Figure 45: Flow Pathlines for Indented Shell at 10m/s

Copyright Applied Research Associates, Inc., 2014

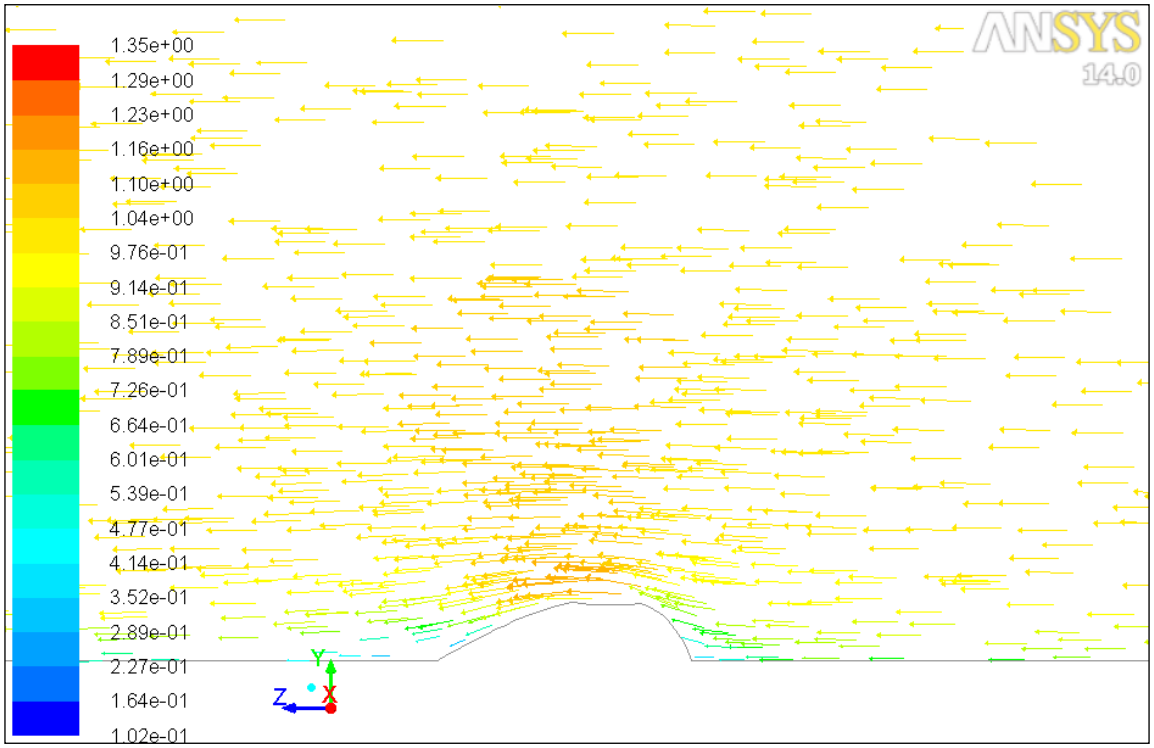

Figure 46: Velocity Vectors for Indented Shell at 10m/s

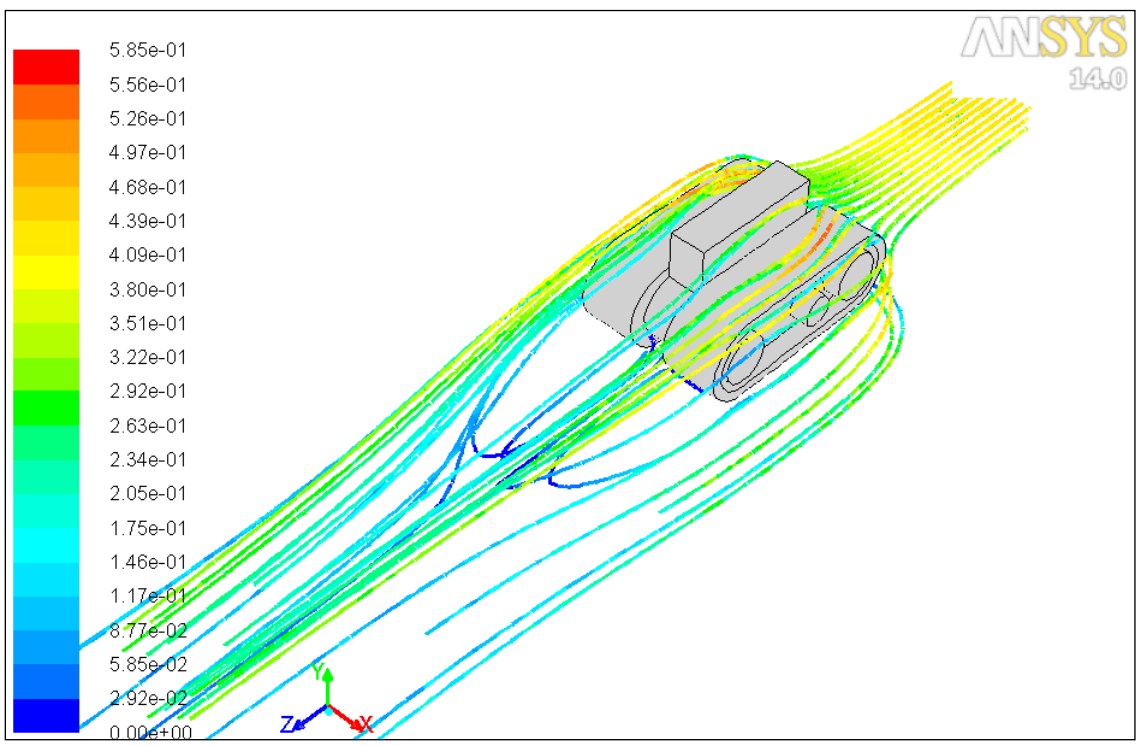

Figure 47: Flow Pathlines for Treaded Vehicle at 0.5m/s

Copyright Applied Research Associates, Inc., 2014

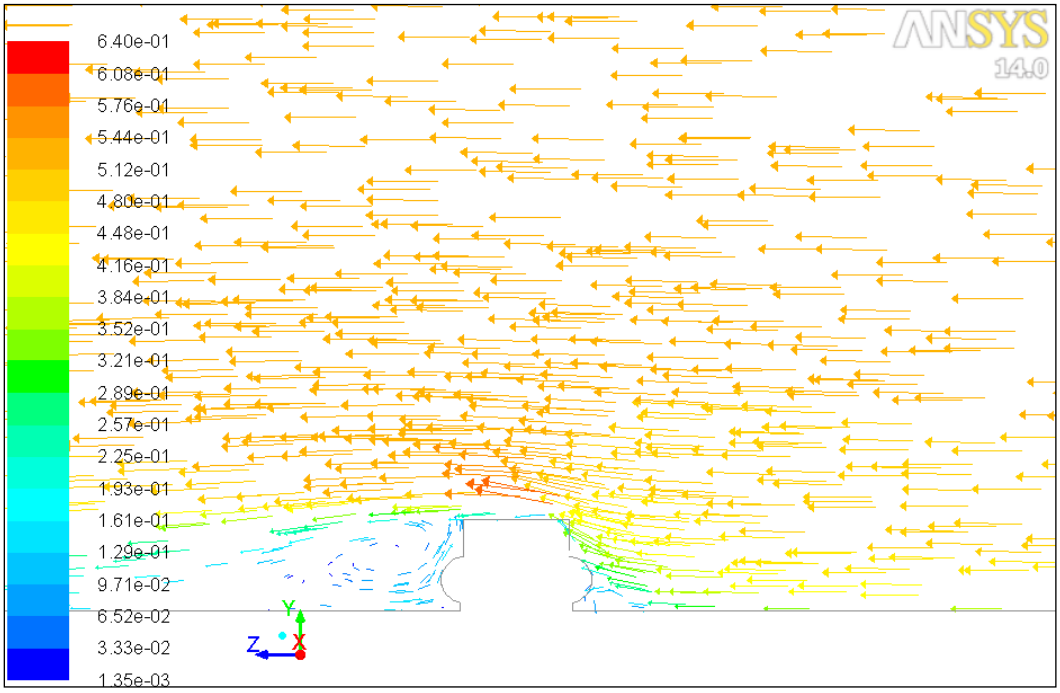

Figure 48: Velocity Vectors for Treaded Vehicle at 0.5m/s

Figure 49 displays data from FLUENT CFD modeling and captures the drag force on every shape tested in the flow velocity range from 0 to 1.5m/s. This is the same range as empirical testing conducted at SIO. The graph shows drag force (Y axis) increasing non-linearly as a function of flow velocity (X axis). This is expected for all shapes tested, but of importance is that the drag force is the lowest for the smooth shell at every velocity tested.

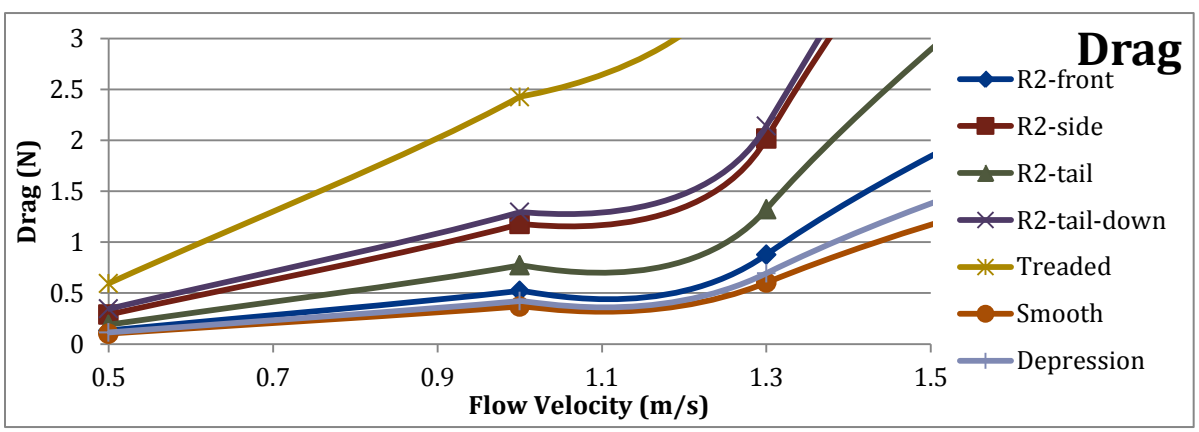

Figure 49: Drag (N) for Four Simulated Models for Flow Velocities from 0 to 1.5m/s

Copyright Applied Research Associates, Inc., 2014

Figure 50 displays data from FLUENT CFD modeling and captures the lift force, which acts normal to the seafloor to dislodge the body, on every shape tested in the flow velocity range from 0 to 1.5m/s. This is the same range as empirical testing conducted at SIO. The graph shows lift force (Y axis) increasing non-linearly as a function of flow velocity (X axis). This is expected for all shapes tested, but of importance is that the lift force for the smooth shell is nearly identical for every shape at every velocity tested. Although, the baseline Horseshoe Crab with tail up had significantly less lift force than the other shapes. This position is not tailored for seafloor travel, drag reduction, and geometric storage efficiency (efficiently SURDP sub-assemblies within the confines of the hull).

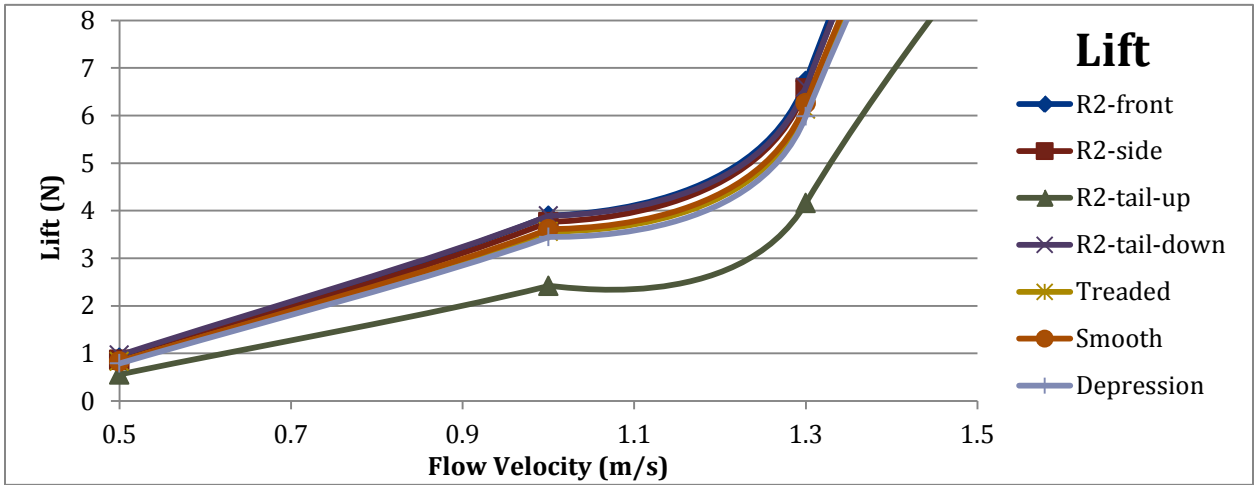

Figure 50: Lift (N) for Four Simulated Models for Flow Velocities from 0 to 1.5m/s

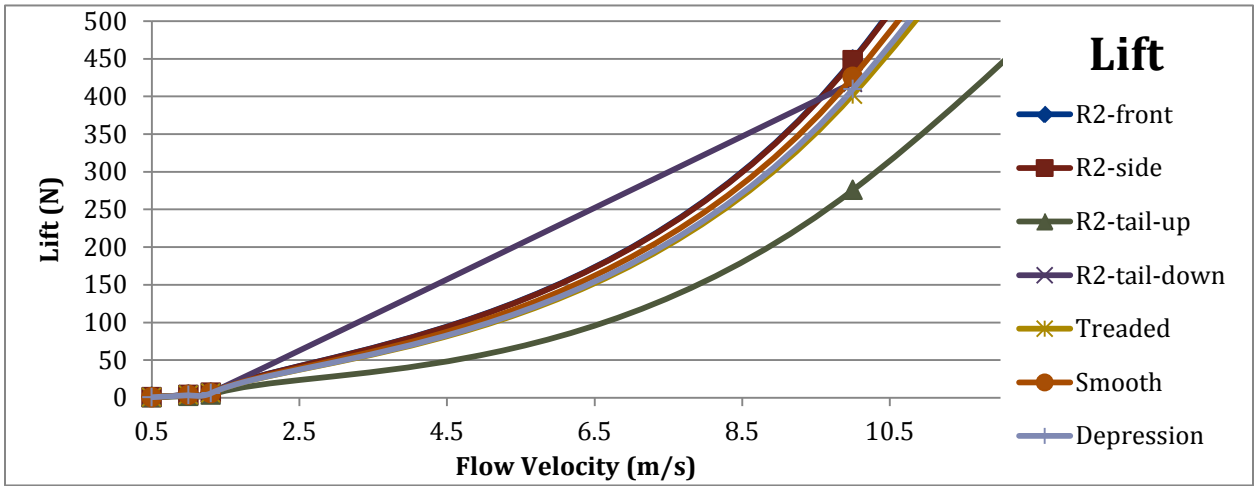

Figure 51: Lift (N) for Four Simulated Models for Flow Velocities from 0 to 10.5m/s

Copyright Applied Research Associates, Inc., 2014

Figure 52 displays data from FLUENT CFD modeling and captures the moment, due to surface drag, which creates a positive moment pushing up on the leading edge of the object. The values are reported as negative due to the axis and direction of applied forces in FLUENT. The flow velocity range is 0 to 25m/s and represents the entire range of simulated velocities. A trendline was fit to the data to further estimate and interpret the results. As flow velocity increases (X axis) the Moment non-linearly increases.

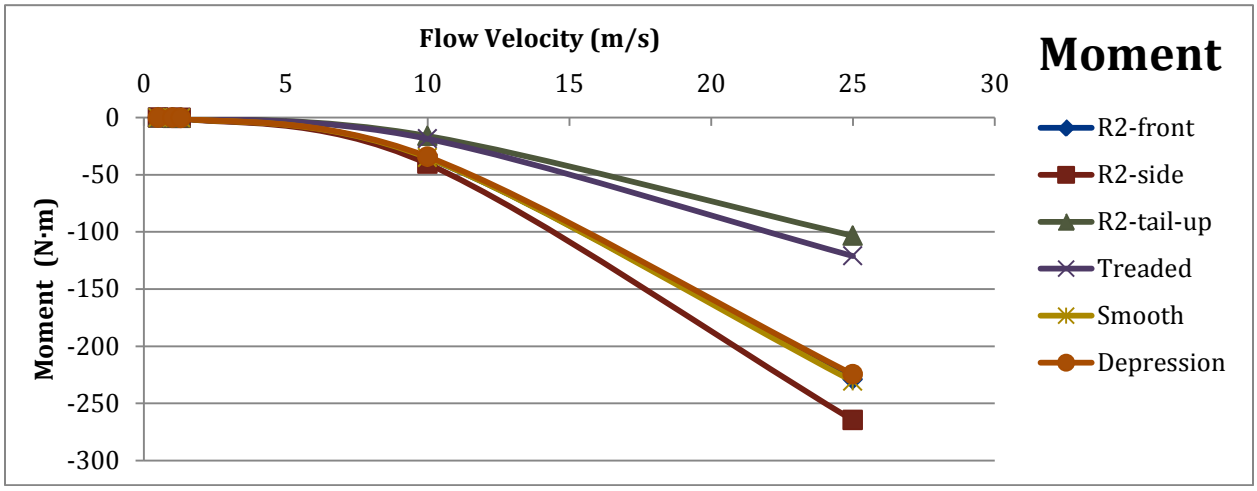

Figure 52: Moment (N•m) for Four Simulated Models at Five Flow Velocities

Figure 52 also displays data from FLUENT CFD modeling and captures the moment, due to surface drag, which creates a positive moment pushing up on the leading edge of the object. The values are reported as negative due to the axis and direction of applied forces in FLUENT. The flow velocity range is only 0 to 1.5m/s. This is the same range as empirical testing conducted at SIO. Although, moment was not empirically tested at SIO for comparison with FLUENT modeling. A trendline was fit to the data to further estimate and interpret the results. As flow velocity increases (X axis) the Moment non-linearly increases.

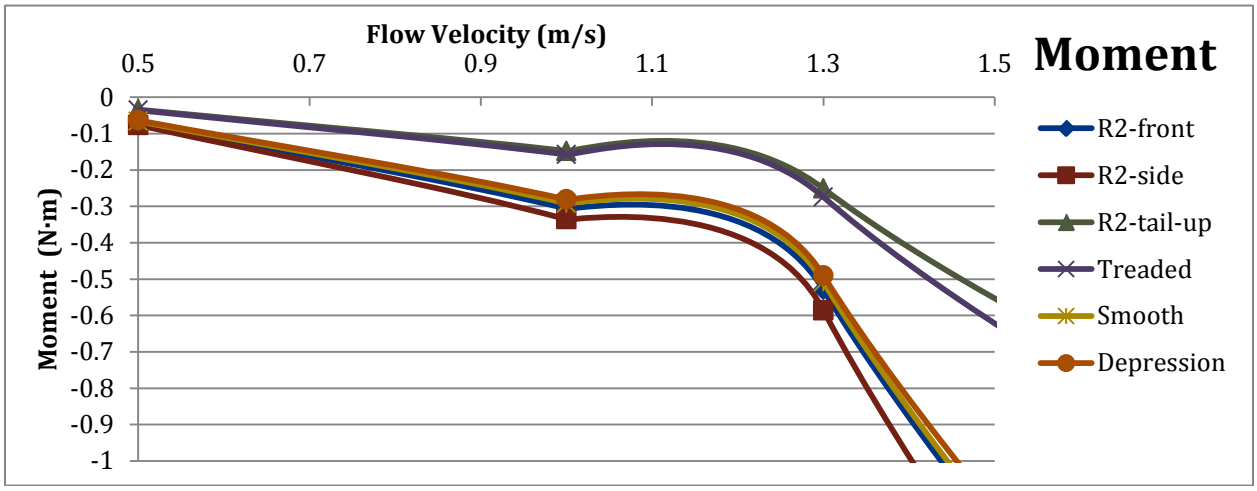

Figure 53: Moment (N•m) for Four Simulated Models for Flow Velocities from 0 to 1.5m/s

Copyright Applied Research Associates, Inc., 2014

Appendix D: Archemedis Screw Test Data

Table 4: Comparison of Fluent CFD and Flow Channel Lift and Drag Coefficients

Model	Velocity	HLab	Fluent	Difference	HLab	Fluent	Difference
	(cm/s)	Cl	Cl	%	Cd	Cd	%
BASELINE	0.5	0.337	0.329	2.318	0.545	0.575	5.460
BASELINE	1	0.294	0.352	19.624	0.561	0.585	4.322
BASELINE	1.3	0.407	0.359	13.279	0.581	0.589	1.380
SMOOTH	0.5	0.246	0.201	22.575	0.117	0.102	14.290
SMOOTH	1	0.210	0.219	4.480	0.093	0.092	1.626
SMOOTH	1.3	0.438	0.224	95.649	0.095	0.089	6.472
DEPRESSION	0.5	0.266	0.191	39.007	0.099	0.117	18.278
DEPRESSION	1	0.198	0.209	5.768	0.130	0.109	19.564
DEPRESSION	1.3	0.228	0.215	5.976	0.100	0.106	5.881

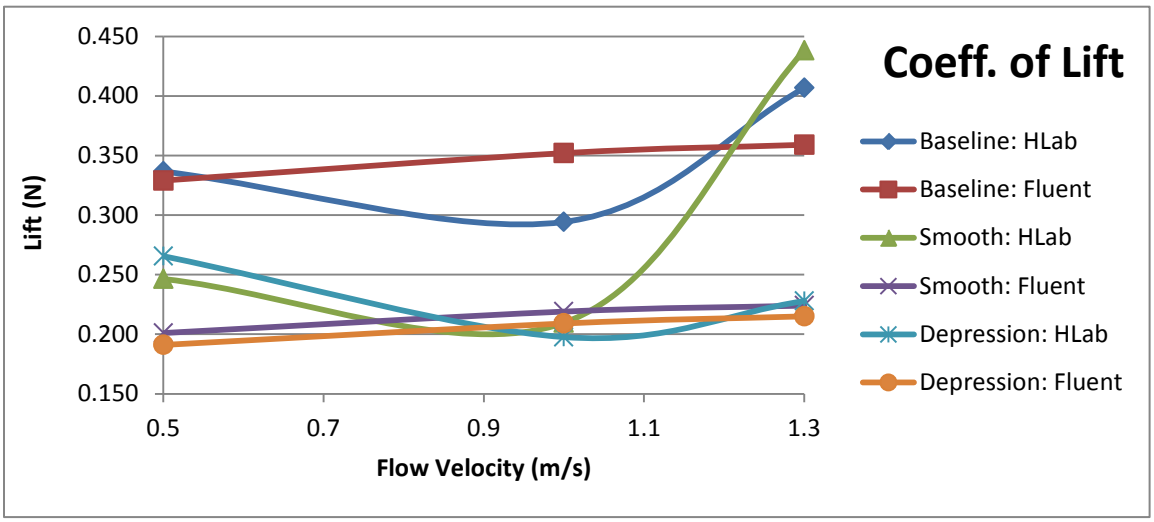

Figure 54: Coefficient of lift for three models at three flow velocities

Copyright Applied Research Associates, Inc., 2014

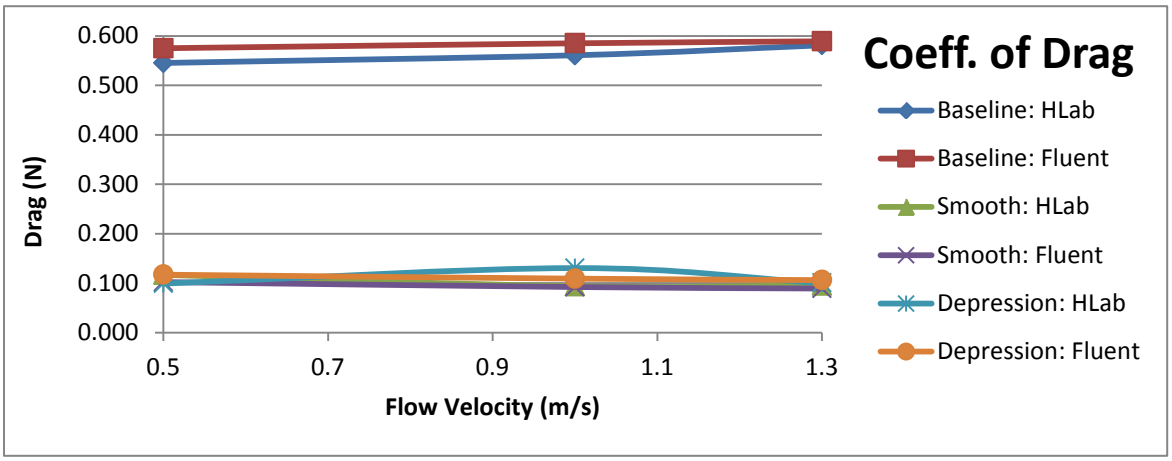

Figure 55: Coefficient of lift for three models at three flow velocities

Copyright Applied Research Associates, Inc., 2014

Appendix E: Archemedis Screw Test Data

Wet Sand

The following table shows the results of the wet sand tests

Table 5: Wet San Test Results

Setup					Results				
Test No.	Screw	Voltage	Platform weight (lbs)	Added weight	Amp Draw	Power Use (Watts)	Average speed Cm/Sec	W*Sec / Meter (N)	Average displacement (cm)
AA	A	7.0V	5.4	0	5-5.3A	36.05	7.149684	504.2181	69
AB	A	11.0V	5.4	0	5.4-5.8A	61.6	15.35764	401.1032	80
AC	A	11.0V	5.4	2 lb	6.5-6.9A	73.7	9.425267	781.9407	46.25
BA	B	7.0V	5.4	0	5.2-5.6A	37.8	7.410977	510.0542	61
BB	B	11.0V	5.4	0	5.8-6.2A	66	13.70138	481.7032	69
BC	B	11.0V	5.4	2 lb	6.5-7A	69.3	4.602872	1505.582	16.5
DA	D	7.0V	5.4	0	3.5-4.0A	26.25	12.02803	218.2402	69
DB	D	11.0V	5.4	0	3.9-4.2A	44.55	21.3843	208.3304	68
DC	D	11.0V	5.4	2 lb	4.8-5.2A	55	18.25747	301.2466	67.5
CA	C	7.0V	5.4	0	4.8-5.1A	34.65	7.813305	443.4743	69
CB	C	11.0V	5.4	0	5.3-5.5A	59.4	13.44456	441.8143	70
CC	C	11.0V	5.4	2 lb	5.9-6.3A	67.1	8.137339	824.5939	28.33

Copyright Applied Research Associates, Inc., 2014

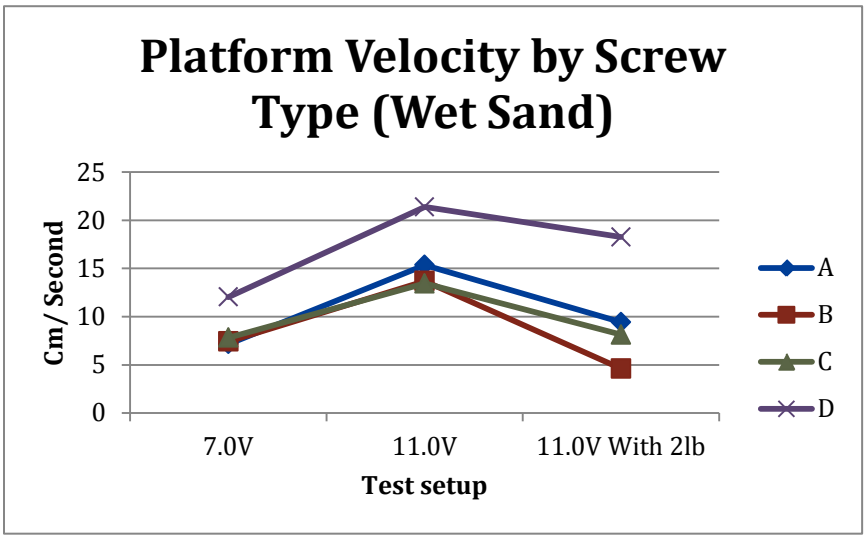

Figure 56: Platform Velocity by Screw Type for Wet Sand

Rock/ Pebbles

The following table shows the test results from running the screws on pebbles.

Table 6: Pebble Test Results

Setup					Results				
Test No.	Screw	Voltage	Platform weight	Added weight	~amp draw	Power Use (Watts)	Average speed Cm/Sec	W*Sec / Meter (N)	Average displacement
AA	A	7.0V	5.4	0	4.5	31.5	6.367076	494.7326	65
AB	A	11.0V	5.4	0	4.7	51.7	12.71367	406.6489	60
AC	A	11.0V	5.4	2 lb	5.3	58.3	3.981089	1464.423	23.6
BA	B	7.0V	5.4	0	4.9	34.3	4.056072	845.6457	34
BB	B	11.0V	5.4	0	4.8	52.8	11.15472	473.342	45
BC	B	11.0V	5.4	2 lb	5.5	60.5	3.520396	1718.556	15.25
DA	D	7.0V	5.4	0	3.6	25.2	10.88445	231.5231	70

Copyright Applied Research Associates, Inc., 2014

DB	D	11.0V	5.4	0	3.8	41.8	18.79953	222.3459	69
DC	D	11.0V	5.4	2 lb	4.2	46.2	15.91595	290.2748	70
CA	C	7.0V	5.4	0	4.6	32.2	4.165707	772.9781	52
CB	C	11.0V	5.4	0	4.7	51.7	8.358483	618.5333	58.7
CC	C	11.0V	5.4	2 lb	5.6	61.6	3.24345	1899.212	18

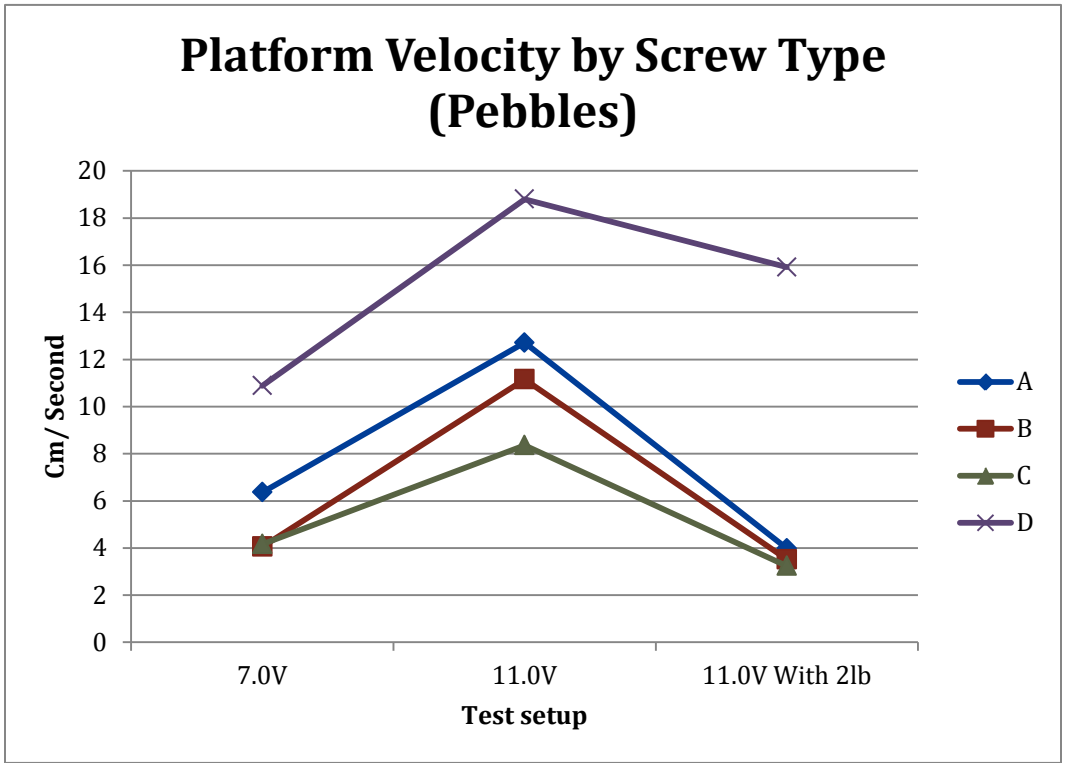

Figure 57: Platform Velocity by Screw Type for Pebbles

Copyright Applied Research Associates, Inc., 2014

Water

The following table shows the results of the water tests.

Table 7: Water Test Results

Setup		Results			
Screw	Voltage	Amp draw	Power Use (Watts)	Average speed Cm/Sec	W*Sec / Meter (N)
A	10.1	2.6	26.26	12.75556	205.8711
B	10.1	2.5	25.25	12.4028	203.5831
C	10.1	2.6	26.26	10.83723	242.3128
D	10.1	2.8	28.28	11.94997	236.6534

Copyright Applied Research Associates, Inc., 2014